UNIVERSITÀ DEGLI STUDI DI MILANO

Facoltà di Scienze e Tecnologie
Laurea Magistrale in Fisica

Classical and Quantum Kinetic Friction Inferred from Equilibrium Properties

Relatore: Prof. Nicola Manini
Correlatore: Prof. Giuseppe Santoro

Mario Forzanini
Matricola n° 46233A
A.A. 2024/2025

Classical and Quantum Kinetic Friction Inferred from Equilibrium Properties

Mario Forzanini
Dipartimento di Fisica, Università degli Studi di Milano,
Via Celoria 16, 20133 Milano, Italia

25 November 2025

Abstract

In the context of the Prandtl-Tomlinson model of atomic friction, we propose a novel semi-quantitative method to predict kinetic frictional properties based on equilibrium averages. We identify the condition for a stick-slip regime with a sufficiently sharp change in the equilibrium free energy as the Prandtl-Tomlinson slider crosses a maximum of the periodic potential, thereby switching from one attraction basin to the next. We apply this method to both the classical and quantum-mechanical model to quantify and compare thermal and tunneling effects on kinetic friction. We find that quantum mechanics affects the sharpness of the free energy exponentially in the opposite of the inverse of the natural parameter for quantumness, in sharp contrast with thermal effects, that decrease the same sharpness proportionally to the inverse temperature.

Relatore: *Prof. Nicola Manini*
Correlatore: *Prof. Giuseppe Santoro*

Chapter 1

Introduction

Which criteria designate a physical phenomenon as worthy of scientific inquiry? In the rest of this introduction we will propose two criteria, and argue that the study of frictional phenomena and in particular *nanofriction*, the topic of this thesis, satisfies both.

A commonly proposed criterion is, of course, the potential technological value one expects to extract from a correct/effective solution of the problem at hand. Evaluating a research topic in this framework amounts to estimating its technological potential, irrespective of its content. In the current context of renewed interest in nanotechnology, nanofriction is a very promising research avenue aimed at understanding the behavior of atomically sized contacts. An accurate modeling of the mechanical properties of nanoscale systems is a crucial step towards engineering them. Indeed, nanotribology has been successfully applied to the study of nanomotors [**?**, **?**], nanoelectromechanical systems [**?**], AFM experiments [**?**, **?**] and contacts between 2D materials [**?**, **?**, **?**, **?**, **?**, **?**, **?**, **?**].

Although scientists are often driven by their intuition about the possible applications of their research, we would argue that scientific inquiry cannot simply be driven by the maximization of likely technological impact. Number theory is a prime example of a case in which such a prediction of technological significance would have been impossible: if mathematical research avenues were ranked based on this criterion alone, the foundation of modern cryptography would not have been developed. Indeed, scientists are often motivated by a deep and possibly inexplicable longing for *beauty*. In the scientific setting beauty is sometimes synonymous with *synthesis*: a beautiful model is one that is able to capture the essence of one or more phenomena, managing to reduce their complexity and capture their intimate essence as much as possible. The research carried out by L. Landau [**?**] is ripe with models with these characteristics, e.g. his work on second-order phase transitions and his introduction of quasiparticles to describe the excitations of many-body systems. The effectiveness of such simple models is in their ability to communicate the key physical characteristics of the phenomena at hand and to predict their broader consequences quantitatively. The value of such a clear intuition of the physical content of any phenomenon vastly exceeds that of any specific technological invention, because it is required before any invention can be attempted.

Even though we are focusing on the aesthetic criteria related to physical

theories and models, the beauty of a model cannot be evaluated irrespective of the physical phenomenon it purports to explain. Beautiful models are such because they efficiently encode physical intuition about *interesting* phenomena, i.e. those that are either very common in nature or especially surprising to the observer, requiring them to change their perspective on the physical world. Sliding friction, in particular, is extremely common in every day life and especially surprising when it comes to its realizations at the micro and nanoscales [**?**]. In this context the frictional properties depend strongly on the atomic configuration and commensurability of the interfaces. The same interface may exhibit radically different properties depending on the orientation [**?**], sliding direction [**?**], speed, and applied load [**?**].

A promising horizon for current research regards the qualitative and quantitative study of new frictional phenomena induced by quantum effects. Although the recent introduction of cold ion traps appears to be a promising field to experimentally probe nanofriction in the quantum regime [**?**], few numerical studies have been conducted [**?**, **?**, **?**] due to the lack of effective computational tools to study quantum dynamics. In this work we propose a new approach based on equilibrium thermodynamics, which allows us to circumvent the generally expensive full dynamical description of kinetic friction in the quantum regime.

In this thesis we study an insightful 1D model proposed nearly a century ago by Prandtl [**?**] and still frequently used today to understand several key features of atomic friction [**?**, **?**, **?**, **?**, **?**]: the so-called Prandtl-Tomlinson (PT) model. This model features a particle interacting with a periodic potential while it is dragged forward through a harmonic spring whose other end (the "slider") advances at constant velocity, see Fig. **??**.

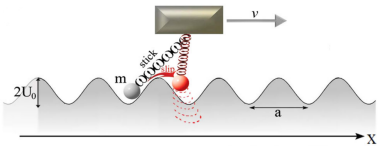

Figure 1.1: Cartoon of the PT model. The PT slider is depicted as a square box pulling the PT particle at constant velocity. Credits: Ref. [**?**].

As detailed in Chap. **??**, the beauty of this model resides in its ability to encode important physical insights about the mechanism for *stick-slip* motion, in few basic mechanical parameters. Stick-slip dynamics, which has broad macroscale evidence e.g. in squeaking breaks and hinges, is a key mechanism accounting for the main component of friction in solid/solid contacts, even at the nanoscale. When stick-slip arises, friction exhibits its full non-linear nature, witnessed by the logarithmic dependence of the average friction force on the sliding velocity [**?**]. After developing our intuition about thermal and quantum effects on stick-slip, we will identify a necessary condition for stick-slip based uniquely on *equilibrium* properties of the model.

The ability to infer properties about kinetic friction from equilibrium quantities is the key idea we propose to carry our classical intuition about stick-slip motion over to the quantum mechanical setting, where fully dynamical simulations are often impractical. In Chap. **??** we will then apply our equilibrium criterion to the quantum PT model and use it to quantify the effect of quantum tunneling on kinetic friction. We find that the effect of quantumness is quite distinct and generally more dramatic than the one of thermal fluctuations.

Chapter **??** draws the conclusions of this research, and outlines its natural extensions, aiming to a better modeling of energy dissipation through the excitation of phonons, rather than via a standard Langevin thermostat.

Appendix **??** reports a low-temperature asymptotic expansion of the classical PT model's partition function referenced in Chap. **??**, Appendix **??** tests the Monte Carlo algorithms described in Chap. **??**, Appendix **??** introduces the shooting method used in Chap. **??** to diagonalize the quantum Hamiltonian of

the PT model. Finally, Appendix **??** lays the foundations for the application of the algorithms described in Chap. **??** to the phonon-coupled PT model.

All of the programs used to generate the figures are available[**?**] under the terms of the GNU General Public License Version 3, or any later version.

Chapter 2

The Prandtl-Tomlinson Model

The simplest and therefore most studied model for sliding friction is the one proposed by L. Prandtl [**?**] in 1928 and historically attributed to both L. Prandtl and G.A. Tomlinson. The qualitative and quantitative insight given by this model still informs the current understanding of dynamical friction nearly a century later. After a brief description of the classical model we introduce and study its quantum mechanical version. In the present Chapter we introduce the classical PT model and review its main features, focusing on the crossover between stick-slip dynamics and smooth-sliding dynamics. We then proceed to formulate a method to predict which of the two can occur, without actually carrying out an explicit dynamical study, but rather focusing on *equilibrium*. We will identify a parameter, named χ and defined below, which needs to be large for stick-slip dynamics to occur at all. Next, by comparing dynamical simulations with equilibrium values of χ, we will nail down the precise range for this parameter.

2.1 The classical PT model

Interest in the classical Prandtl-Tomlinson [**?**] model stems from its ability to describe and characterize stick slip motion as the main contributor to sliding friction. The model is one dimensional and it consists of a particle of mass M at position X, interacting with a static periodic potential and a harmonic spring dragged with constant velocity $\tilde{v}$. The particle is furthermore coupled to an environment acting as an energy sink and modeled as a viscous force $-M\Gamma\dot{X}$. The equation of motion reads [1] :

$$M\ddot{X} = -M\Gamma\dot{X} - \frac{\partial}{\partial X}\left[\frac{K}{2}(X-\tilde{X})^2 + V_0\cos\left(\frac{2\pi}{a}X\right)\right], \quad \tilde{X} = \tilde{v}t. \tag{2.1}$$

In the following we will refer to $\tilde{X}$ as the position of the slider and to the term in brackets as the classical PT potential $V_{\mathrm{PT}}(X;\tilde{X})$. The main parameter that influences the dynamics of the system is the ratio between the curvature of the sinusoidal potential at its minimum $4\pi^2V_0/a^2$ and the harmonic spring constant K:

$$\eta = \frac{4\pi^2V_0}{Ka^2}. \tag{2.2}$$

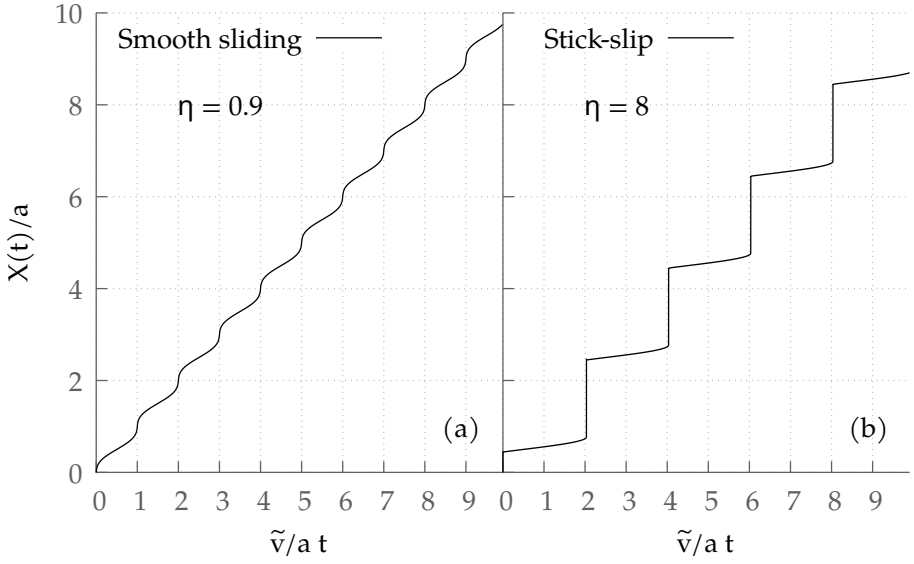

Figure 2.1: Prototypical examples of time evolution $X(t)$ at zero temperature $T = 0\,\mathrm{K}$. Panel (a): an example of smooth-sliding dynamics ($\eta = 0.9$); panel (b): an example stick-slip dynamics ($\eta = 8$). See Section **??** below for details on the algorithm employed, and Fig. **??** for the whole set of parameters adopted.

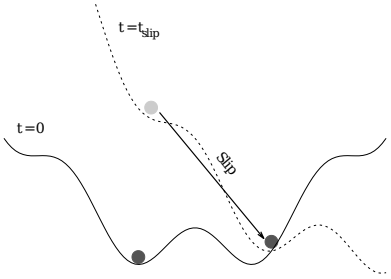

Figure 2.2: Cartoon of the "slip" event. The solid and dashed curves represent the Prandtl-Tomlinson potential energy surface $V_{\mathrm{PT}}(X; \tilde{X} = \tilde{v}t)$

When $\eta < 1$ the sinusoidal potential acts as a relatively weak perturbation to the spring energy: as a result the particle is dragged along with the spring, in a regime usually termed *smooth sliding*, Fig. **??**a. On the other hand, when $\eta > 1$ the system can experience *stick-slip motion*, see Fig **??**b, which is characterized by two phases: an energy accumulation process in which the system is stuck near a local minimum, the "stick" phase, followed by a sudden release of the accumulated energy with a leap into a successive energy minimum, the "slip" phase (see Fig. **??** for a pictorial representation).

2.2 Langevin Dynamics

In this section, after establishing an intuitive picture of stick-slip motion as caused by the formation of transient energy barriers that weaken and eventually vanish, we will study the dependence of stick-slip on simulation parameters Γ, $\tilde{v}$, T and η.

Before any discussion of stick-slip, let us introduce appropriate dimensionless variables in the equation of motion Eq. (**??**). The periodicity of the potential suggests to use the lattice spacing a as unit of length and

$$\nu_a^{-1} = a/\tilde{v} \tag{2.3}$$

as unit of time ($\nu_a = \tilde{v}/a$ is usually called *washboard frequency*). We furthermore introduce the *critical damping*:

$$\Gamma_c = 2\sqrt{\frac{K}{M}}, \tag{2.4}$$

which separates the overdamped regime $\Gamma > \Gamma_c$ from the underdamped one $\Gamma < \Gamma_c$. This definition focuses on the damping properties of the driving spring, which is the slowest mode in the model's interesting regime $\eta > 1$ compatible

Dimensionless quantity	Definition
PT ratio η	$\eta = \dfrac{4\pi^2 V_0}{K a^2}$
damping ratio γ	$\gamma = \dfrac{\Gamma}{\Gamma_c} = \dfrac{\Gamma}{2\nu_K}$
slider speed s	$s = \dfrac{\nu_a}{\nu_K}$
time τ	$\tau = \nu_a t = \dfrac{\tilde{v} t}{a}$
slider's position $\tilde{x}$	$\tilde{x} = \dfrac{\tilde{X}}{a} = \dfrac{\tilde{v} t}{a} = \tau$
PT particle's position x	$x = \dfrac{X}{a}$

Table 2.1: Dimensionless model parameters, plus the dimensionless time τ and position x. Here $\nu_K = \sqrt{K/M}/(2\pi)$ is the oscillator frequency associated to the driving spring, and $\nu_a = \tilde{v}/a$ is the washboard frequency associated to the advancing slider.

with stick-slip. A stick-slip regime differentiates better from smooth sliding in the underdamped dynamics where the slip phase is not significantly slowed down by viscous friction. In practice therefore we will focus on $\Gamma < \Gamma_c$. We introduce a dimensionless damping ratio

$$\gamma = \frac{\Gamma}{\Gamma_c} < 1\,. \tag{2.5}$$

The third and last parameter relates the speed of the slider to the typical oscillation frequency in the minimum of the driving spring's potential well:

$$s = \frac{\nu_a}{\nu_K} = \frac{2\pi}{a\sqrt{K/M}}\,\tilde{v}, \tag{2.6}$$

$$\nu_K = \frac{1}{2\pi}\sqrt{\frac{K}{M}}. \tag{2.7}$$

When all other parameters are fixed, changing s amounts to modifying the PT model driving speed $\tilde{v}$.

Introducing the dimensionless position $x = X/a$ and dimensionless time $\tau = \nu_a t$, the equation of motion reads:

$$\frac{\mathrm{d}^2 x}{\mathrm{d}\tau^2} = -4\pi\frac{\gamma}{s}\frac{\mathrm{d}x}{\mathrm{d}\tau} + \frac{4\pi^2}{s^2}\left[\tau - x + \frac{\eta}{2\pi}\sin(2\pi x)\right]. \tag{2.8}$$

Table **??** summarizes the dimensionless quantities of the model.

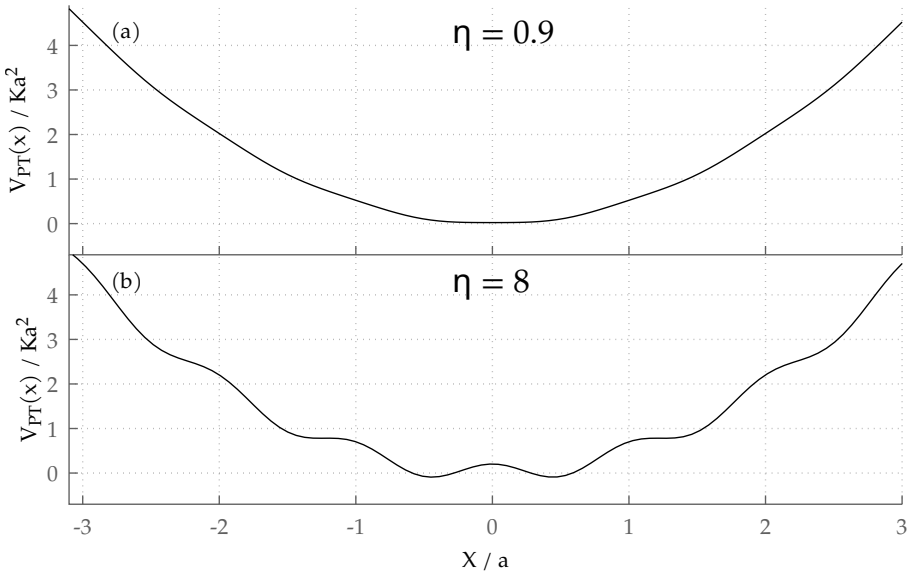

Figure 2.3: Potential energy for the PT model $V_{PT}(X;\tilde{X}=0)$ for (a) $\eta = 0.9 < 1$ and (b) $\eta = 8 > 1$. The possibility of stick-slip in the $\eta > 1$ region is related to the competition between multiple potential-energy minima.

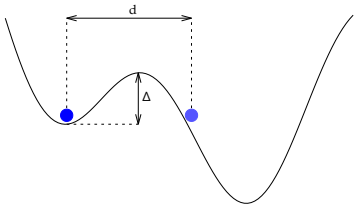

Figure 2.4: Cartoon of the energy barrier Δ that causes the stick phase.

Stick-slip can only occur for $\eta > 1$, which corresponds to the formation of multiple coexisting potential-energy minima, see Fig. **??**. Indeed, during the dynamics the presence of an energy barrier $\Delta(t)$ between the occupied local minimum and the global one causes the particle to "stick" in the unfavorable position, while the vanishing of such barrier at a specified time t_{slip}, $\Delta(t_{slip}) = 0$,

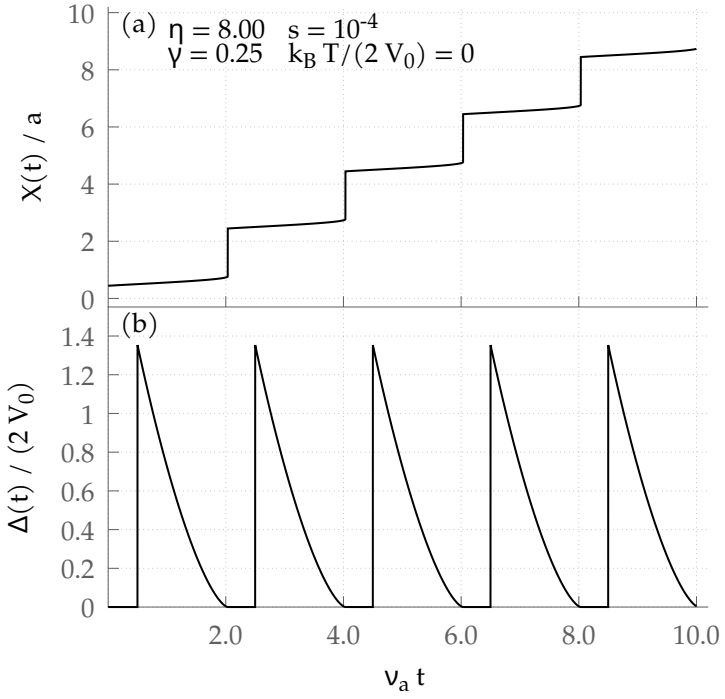

Figure 2.5: Panel (a) typical example of stick-slip time evolution $X(t)$, Panel (b) energy barrier $\Delta(t)$, see Fig. **??**. Clearly, the slip event coincides with the vanishing of $\Delta(t)$.

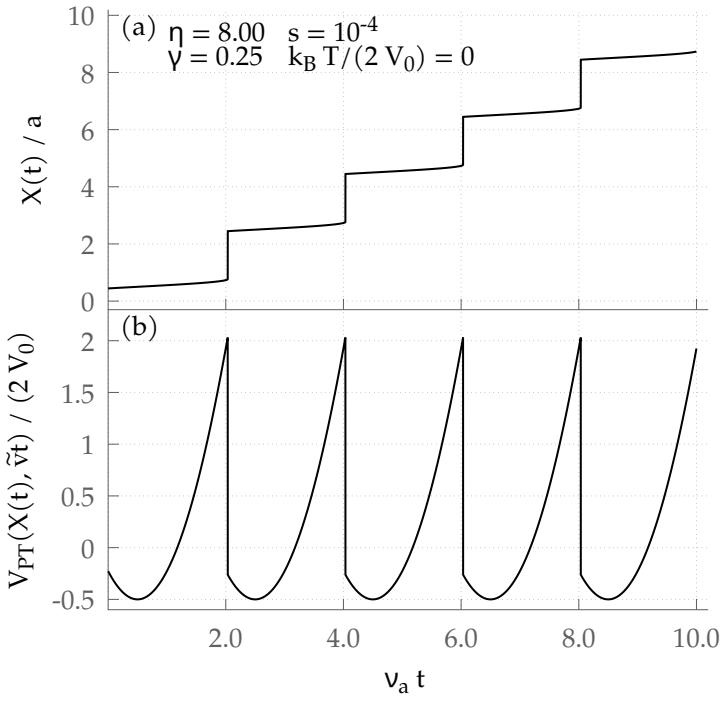

el (a) typical example evolution $X(t)$, Panel nergy $V_{PT}(X(t), \tilde{v}t)$. corresponds to an en- on process that culmi- dissipation during the

allows the particle to "slip" into a more favorable configuration, see Figs. **??** and **??**. The energy accumulated during the stick phase is transferred to the environment during the slip, thus accounting for the highly dissipative nature of stick-slip dynamics.

Qualitative parameter dependence of stick-slip

The existence of stick-slip motion depends non-trivially on the parameters of the model and a quantitative description can only be achieved via computer simulation, nonetheless we attempt to give a qualitative description that will guide our simulations.

For simplicity, let us first focus on the $T = 0$ case, where the dependence on the energy is simple: stick-slip can only happen for $\eta > 1$. Suppose we fix $\eta > 1$, our pictorial understanding of stick-slip is based on the occasional inability of the PT particle to overcome potential energy barriers. This picture suggests that for a sufficiently fast sliding velocity, the particle will have no time to stick into the minimum, i.e. for

$$\frac{1}{2}M\tilde{v}^2 \gg 2V_0, \tag{2.9}$$

stick-slip will be suppressed by inertia. This suppression of stick-slip occurs continuously, as analyzed in detail in Ref. [**?**], across an upper crossover slider velocity $v_c^u(T = 0, \eta, \gamma)$ above which the system will experience smooth sliding, see Fig. **??**. Similarly we we expect temperature to *preempt* the energy barriers by thermally hopping over them. As a result an increase in temperature tends

vay by which iner- or $\tilde{v} > v_c^u(T, \eta, \gamma)$.

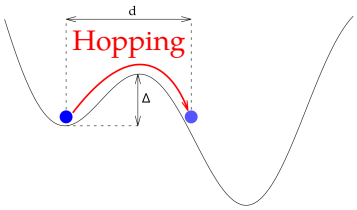

Figure 2.8: Cartoon of a thermally activated barrier hopping event.

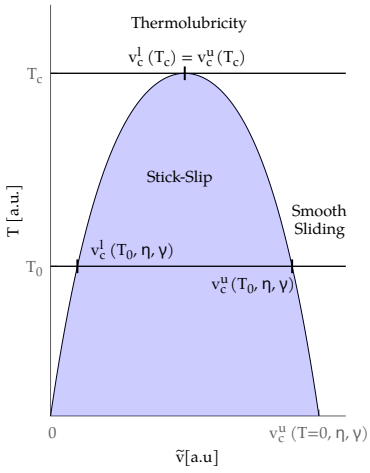

Figure 2.9: Cartoon of the expected boundary separation between stick-slip and thermolubric/smooth-sliding phases.

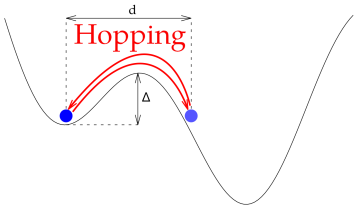

Figure 2.10: Cartoon of the diffusive motion typical of *thermolubricity*.

to favor smooth sliding against stick-slip, thus reducing the upper crossover velocity

$$\frac{\mathrm{d}v_c^u(T,\eta,\gamma)}{\mathrm{d}T} < 0. \tag{2.10}$$

On the other hand, for any nonzero temperature, diffusion will let the system overcome any barrier, provided that we allow it long enough. This suggests that if the slider advances sufficiently slowly the particle has a chance to thermally hop back-and-forth over the barrier. This low-speed diffusive regime terminates the stick-slip phase at a lower critical slider velocity $v_c^l(T,\eta,\gamma)$ below which stick-slip cannot occur. As temperature increases [**?**] the time τ_T required to hop over a barrier of size Δ, see Fig. **??**, decreases exponentially:

$$\tau_T \propto f^{-1} \exp\left(\frac{\Delta}{k_B T}\right), \tag{2.11}$$

with f the attempt frequency. If we take the distance between the minima separated by the barrier to be d, see Fig. **??**, and the speed of the particle to be v, then the time needed to overcome the barrier "dynamically" τ_v is of the order of:

$$\tau_v \propto \frac{d}{v}. \tag{2.12}$$

In the case of the PT system we can take $d \sim a, \Delta \sim 2V_0$ and expect the crossover velocity v_c^l to correspond to the matching between τ_T and τ_v:

$$v_c^l(T) \propto af \exp\left(-\frac{2V_0}{k_B T}\right). \tag{2.13}$$

So we expect the lower critical velocity to increase with temperature:

$$\frac{\mathrm{d}v_c^l(T,\eta,\gamma)}{\mathrm{d}T} > 0, \tag{2.14}$$

and most importantly we know that this effect does not happen at $T = 0$, so that:

$$\lim_{T\to 0} v_c^l(T,\eta,\gamma) = 0. \tag{2.15}$$

The combination of Eqs. (**??**),(**??**) suggests that there exists a sufficiently high temperature $T_c(\eta,\gamma)$ such that:

$$v_c^l(T_c(\eta,\gamma),\eta,\gamma) = v_c^u(T_c(\eta,\gamma),\eta,\gamma), \tag{2.16}$$

and for any temperature $T > T_c$ no stick-slip can occur, see Fig. **??**. In this regime, usually termed *thermolubricity*, thermal fluctuations are so large that both forward and backward barrier hopping can occur and stick-slip cannot be meaningfully defined, see Fig. **??**.

If we now consider how temperature will affect the energetics of the system, as we remarked above we expect the primary thermal effect to be a reduction of effective barriers, so that we expect the necessary condition $\eta > 1$ to be weakened to $\eta > \eta_c(T) \geq 1$. After guessing the expected shape of the "phase diagram" of this system as a function of η, T and $\tilde{v}$, let us report our results obtained via MD simulations.

How to recognize Stick-Slip automatically

In this section we will discuss the algorithms we implemented[**?**] in order to obtain a diagram similar to Fig. **??** via MD simulations.

First of all, we need to simulate the dynamics of the PT system at $T > 0$. We do so by integrating the Langevin equation:

$$\begin{cases} \frac{\mathrm{d}X(t)}{\mathrm{d}t} & = V(t), \\ M\frac{\mathrm{d}V(t)}{\mathrm{d}t} & = -\frac{\partial V_{\mathrm{PT}}(X,t)}{\partial X} - M\Gamma V(t) + W(t) \\ X(0) & = X_0, \\ V(0) & = V_0, \end{cases} \tag{2.17}$$

where $W(t)$ is a Gaussian noise term representing the thermal random force applied by the thermostat, and is chosen so that it satisfies the fluctuation-dissipation theorem:

$$\begin{aligned} \langle W(t)\rangle &= 0, \\ \langle W(t)W(t')\rangle &= 2M\Gamma k_{\mathrm{B}}T\delta(t-t'). \end{aligned} \tag{2.18}$$

Following a procedure similar to that used for Eq. (**??**), we proceed then to express Eq. (**??**) in terms of the previously defined dimensionless constants η, γ, s and dynamical variables x, τ etc. (see Table **??**):

$$\begin{cases} \frac{\mathrm{d}x(\tau)}{\mathrm{d}\tau} & = v(\tau), \\ \frac{\mathrm{d}v(\tau)}{\mathrm{d}\tau} & = \frac{4\pi^2}{s^2}\left[\tau - x + \frac{\eta}{2\pi}\sin(2\pi x)\right] - \frac{4\pi\gamma}{s}v(\tau) + w(\tau), \\ x(0) & = x_0, \\ v(0) & = v_0, \end{cases} \tag{2.19}$$

with $w(t) = W(t)/(Ma^2\nu_a^2)$. In order integrate this equation we implement[**?**] the simple Grønbech-Jensen-Farago [**?**] algorithm: we fix an integration timestep $\mathrm{d}\tau$ and approximate the discretized positions $x_n \simeq x(n\mathrm{d}\tau)$, $n \in \mathbb{N}$, and velocities $v_n \simeq v(n\mathrm{d}\tau)$ by evolving the initial conditions according to the GJF equations:

$$\begin{cases} x_{n+1} & = x_n + b\mathrm{d}\tau w_n + \frac{2\pi^2 b\mathrm{d}\tau^2}{s^2}f_n + \frac{2\pi^2 b\mathrm{d}\tau}{s^2}w_{n+1}, \\ v_{n+1} & = v_n + \frac{2\pi^2\mathrm{d}\tau}{s^2}(f_n + f_{n+1}) - \frac{4\pi\gamma}{s}(x_{n+1} - x_n) + \frac{4\pi^2}{s^2}w_{n+1}, \end{cases} \tag{2.20}$$

where w_n is a random number sampled from a Gaussian distribution:

$$\begin{aligned} \langle w_n\rangle &= 0, \\ \langle w_n w_l\rangle &= \frac{\gamma}{\pi^3}s\eta\frac{k_{\mathrm{B}}T}{2V_0}\mathrm{d}\tau\delta_{n,l}, \end{aligned} \tag{2.21}$$

the discretized dimensionless forces f_n are:

$$f_n = n\mathrm{d}\tau - x_n + \frac{\eta}{2\pi}\sin(2\pi x_n) \tag{2.22}$$

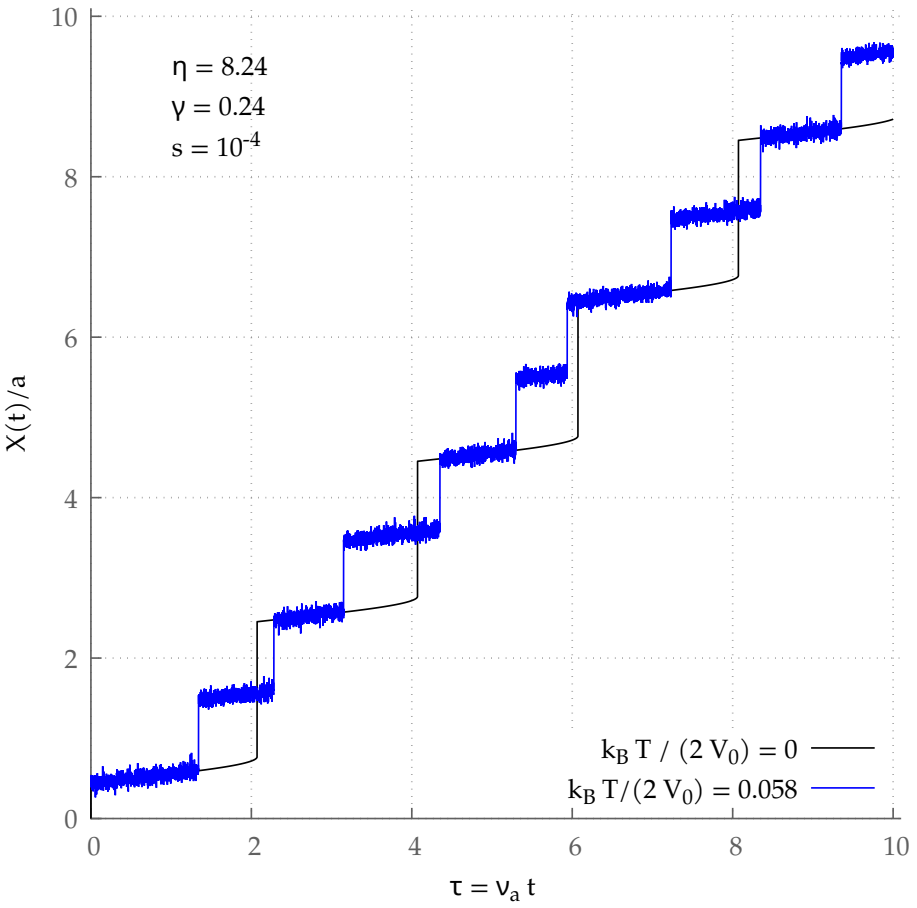

Figure 2.11: Examples of time evolution $x(\tau)$ in the stick-slip regime. The parameters are taken from Ref. [**?**]: $V_0 = 0.22\,\text{eV}$, $a = 0.315\,\text{nm}$, $K = 1.71\,\text{N/m}$, $M = 2.84 \times 10^{-9}\,\text{kg}$, $T = 300\,\text{K}$, $\Gamma = 1.169 \times 10^{4}\,\text{s}^{-1}$. In this example the dynamics switches from multiple-slip at $T = 0$ to single-slip at $k_\text{B}T = 300\,\text{K}$, i.e. $k_\text{B}T/(2V_0) = 0.058$.

and

$$b = \frac{1}{1 + \frac{2\pi\gamma \mathrm{d}\tau}{s}}. \tag{2.23}$$

To show the effect of temperature on a stick-slip, in Fig. **??** we display a particularly stark example of a temperature-induced transition from double-slip to single-slip.

In order to obtain a diagram similar to Fig. **??**, we need to come up with an algorithm to reliably post-process a trajectory and detect the presence or absence of stick-slip events. We propose the following approach:

- Integrate the Langevin equation Eq. (**??**) to compute the trajectory of the PT particle $x(\tau)$,
- Discard an initial transient $\tau_\text{transient}$,
- Fix a time interval $\Delta\tau$ larger than the duration of a slip and shorter than the length of a period, i.e. 1 in our units, and compute the *jump*:

$$\Delta x(\tau, \Delta\tau) = x(\tau) - x(\tau - \Delta\tau), \tag{2.24}$$

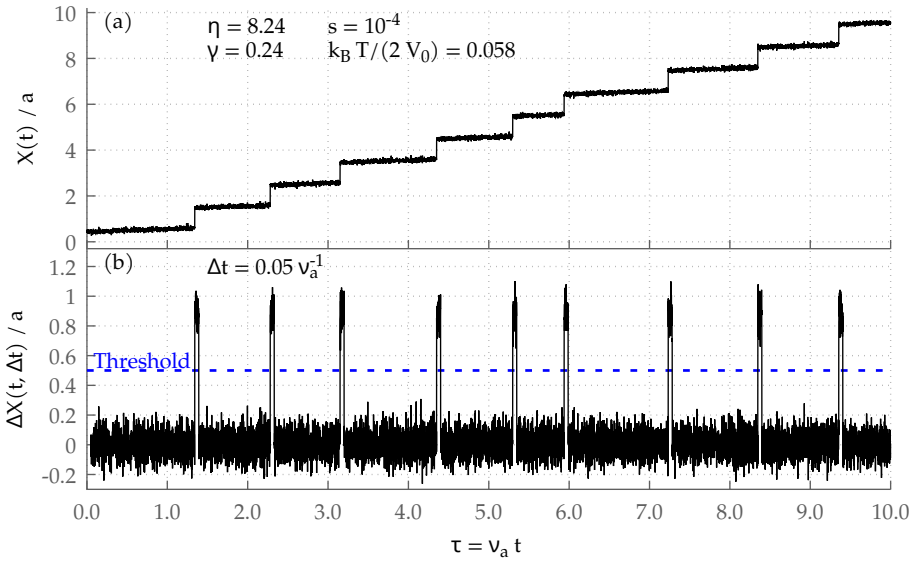

Panel (a): Same as b): Jump $\Delta X(t, \Delta t =$.

- When at any time the jump $\Delta x(\tau, \Delta\tau)$ is sufficiently wide, we have a clear indication of a transition between two wells, see Fig.**??**; instead, a large negative $\Delta x(\tau, \Delta\tau)$ signals a backward transition. In particular, jumps $\Delta x(\tau, \Delta\tau)$ are considered to be sufficiently wide if they cross a threshold: $|\Delta x(\tau, \Delta\tau)| > \mathcal{T}$, which we take to be $\mathcal{T} > 0.5$ to distinguish forward and backward jumps from thermal noise.

Unfortunately, neither the transition to smooth sliding in the high velocity range, $v \simeq v_c^u$, nor the transition to the thermolubric regime in the high temperature range, $T \simeq T_c$, are sharp. In the regions of parameter space close to the transition it is particularly hard to meaningfully classify trajectories. In order to work around this problem we classify trajectories into three categories: *stick-slip*, *not stick-slip* and *crossover*, see Fig. **??** for examples.

Before presenting our results we discuss the criteria we used to classify the trajectories. Let us denote by N the number of time steps in the trajectory and by $N_{<0}$ and $N_{>0}$ the number of points such that $\Delta x(\tau, \Delta\tau)$ falls below $-\mathcal{T}$ or above $\mathcal{T}$, respectively. Similarly we will denote by $\tau_{>0}$ and $\tau_{<0}$ the sets of time steps τ such that $\Delta x(\tau, \Delta\tau) > \mathcal{T}$ and $\Delta x(\tau, \Delta\tau) < -\mathcal{T}$, respectively. We identify 4 criteria that can be tested to reasonably classify a trajectory as *not stick-slip*:

- $|\Delta x(\tau, \Delta\tau)| < \mathcal{T}$: there are no jumps between potential energy minima,
- For a given $\Delta\tau$ any slip event shorter than $\Delta\tau$ will correspond to a window of $\lfloor \Delta\tau/\mathrm{d}\tau \rfloor$ values such that $\Delta x(\tau, \Delta\tau) > \mathcal{T}$. So if:

$$\frac{N_{>0}}{\lfloor \Delta\tau/\mathrm{d}\tau \rfloor} \ll N\mathrm{d}\tau \tag{2.25}$$

  we consider the recognized slip events as accidental[2]. This may happen when $\Delta x(\tau, \Delta\tau) \lesssim \mathcal{T}$ and it accidentally crosses the threshold $\mathcal{T}$.
- If the standard deviation $\sigma(\Delta x)$ is above the threshold: $\sigma(\Delta x) > \mathcal{T}$, we consider the trajectory to be in the thermolubric regime, like Fig. **??**c.

nits $\tilde{v} = 1$, so umber of wave- der.

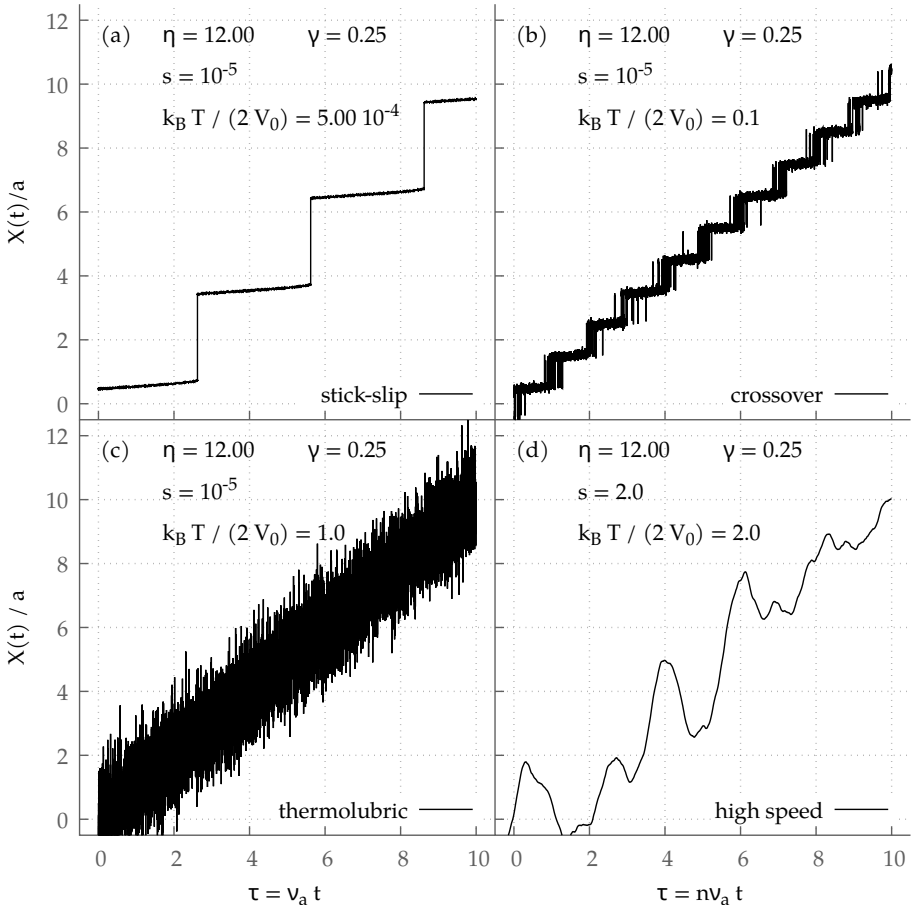

Figure 2.13: Examples of MD trajectories for the PT model, at $\eta = 12$, $\gamma = 0.25$, and (a): $s = 10^{-5}$, $\overline{T} = k_B T/(2V_0) = 5 \times 10^{-4}$; (b): $s = 10^{-5}$, $\overline{T} = 10^{-1}$; (c): $s = 10^{-5}$, $\overline{T} = 1$; (d): $s = 2$, $\overline{T} = 2$. Note how both trajectories in panel (b) and panel (d) show features of stick-slip motion and thermolubric-like backward jumps. Assigning a label to these trajectories is practically arbitrary.

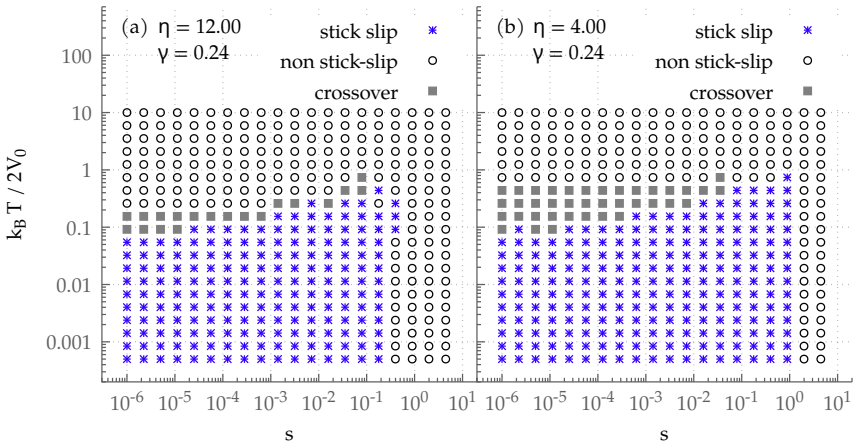

Figure 2.14: Diagram of the stick-slip "phase" as a function of speed s and temperature $k_B T/(2V_0)$. Integration timesteps range from $d\tau = 10^{-8}$ for $s \lesssim 10^{-5}$ to $d\tau = 10^{-6}$ for $s \gtrsim 10^{-4}$, while $\Delta\tau$ ranges from $\Delta\tau = 0.01$ to $\Delta\tau = 1$ and thresholds $\mathcal{T}$ range from $\mathcal{T} = 0.5$ to $\mathcal{T} = 2$.

- Similarly, if the root mean displacement of the negative jumps crosses the threshold:
$$\mathrm{RMSD}(\Delta x(\tau_{<0}, \Delta\tau)) > \mathcal{T}, \tag{2.26}$$
we consider the trajectory to be in the thermolubric regime.

If none of the above criteria applies to the trajectory, we classify it as *undecided* if one of the following is true:

- $N_{<0}$ is comparable to $N_{>0}$:
$$N_{<0} > p_1 N_{>0}, \tag{2.27}$$
for a given fraction $p \approx 1$, which we set to be $p_1 = 0.8$. This criterion should identify situations similar to Fig. **??**b.

- If the number of positive peaks is greater than the number of periods:
$$\frac{N_{>0}}{\lfloor \Delta\tau / \mathrm{d}\tau \rfloor} > p_2 N \mathrm{d}\tau, \tag{2.28}$$
for some $p_2 > 1$, and the number of negative peaks is comparable to the number of positive ones:
$$\frac{N_{<0}}{N_{>0}} > p_3, \tag{2.29}$$
for some $p_3 \lesssim 1$. We take $p_2 = 1.5$ and $p_3 = 0.8$ in our simulations.

Our units are chosen to ensure that $\tilde{v} = 1$, so MD trajectories will be comparable across a wide range of parameter values s, T, η, γ. Simulation results are shown in Fig. **??**, which displays a "phase diagram" similar to the cartoon in Fig. **??**. For both $\eta = 12$, Fig. **??**a, and $\eta = 4$, Fig. **??**b, stick-slip seems to disappear for any temperature $k_\mathrm{B}T/(2V_0) > 1$.

2.3 Equilibrium signature of stick-slip dynamics

At zero temperature, the “stick" phase is the result of the presence of multiple competing energy minima at any fixed time, with the particle remaining stuck in one of them. The “slip" takes place when the particle overcomes the barrier and hops into an energetically more favorable minimum nearby. The effect of temperature is then to preempt the “stick” by thermally hopping over the barrier. The probability of hopping raises as the slider velocity decreases. In the adiabatic limit of ultralow-velocity $\tilde{v} \to 0$, stick-slip is replaced by random diffusive back-and-forward jumps across the barrier. In this limit the slider's position is essentially constant, while the particle explores configurations weighted according to the quasi-equilibrium Boltzmann distribution $\exp\big(-\beta H(P, X, \tilde{X})\big)$. From the point of view of an external experimenter moving the slider is equivalent to exploring the free-energy landscape:

$$\begin{aligned} F(\tilde{X}) &= -k_\mathrm{B}T \log\big(Z(\tilde{X})\big), \\ Z(\tilde{X}) &= \int \frac{\mathrm{d}X \mathrm{d}P}{2\pi\hbar} \mathrm{e}^{-\beta\left(\frac{P^2}{2M} + V_\mathrm{PT}(X, \tilde{X})\right)} \\ &= \int \frac{\mathrm{d}X}{\Lambda} \exp\big(-\beta V_\mathrm{PT}(X, \tilde{X})\big), \end{aligned} \tag{2.30}$$

where Λ is the thermal length defined by:

$$\frac{k_B T}{4\pi} = \frac{\hbar^2}{2M\Lambda^2} \implies \Lambda = \sqrt{\frac{\hbar^2 \beta 2\pi}{M}}. \tag{2.31}$$

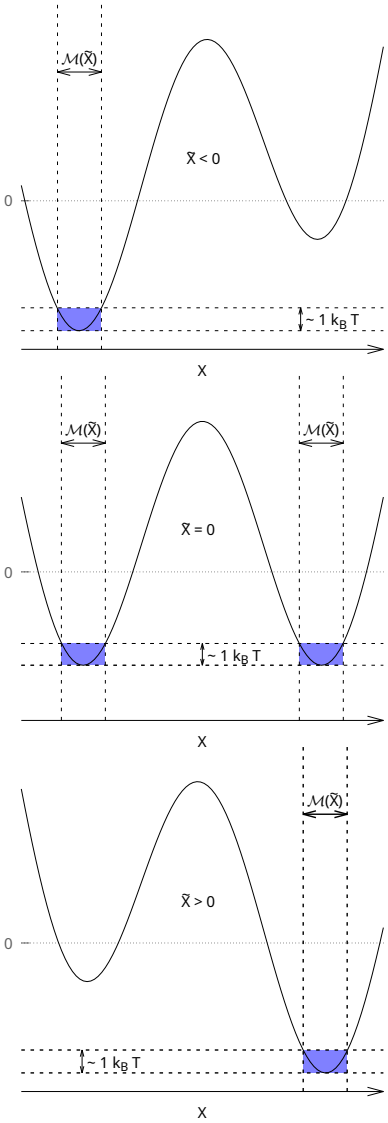

Figure 2.15: A cartoon representing the set of dominant points $\mathcal{M}(\tilde{X})$ for a low temperature, $k_B T/(2V_0) \ll 1$.

In concrete, to keep the slider's velocity constant, the instantaneous external force has to be equal and opposite to the average force

$$\mathcal{F} = \left\langle -\frac{\partial V_{\mathrm{PT}}(X, \tilde{X})}{\partial \tilde{X}} \right\rangle = -\frac{\partial F(\tilde{X})}{\partial \tilde{X}} \tag{2.32}$$

generated by the Prandtl-Tomlinson particle. For any fixed slider position $\tilde{X}$, the exponential decay of the Boltzmann weight $\exp\left(-\beta V_{\mathrm{PT}}(X, \tilde{X})\right)$ implies that any thermal average will be determined by the configurations within a few multiples of $k_B T$ from the global potential energy minima. The presence of energy barriers between competing potential energy minima, a necessary condition for stick-slip, will then reflect in the average force as follows. Provided that the temperature is low enough to neglect the weight of configurations with energy close to the barrier height, i.e. $k_B T \ll 2V_0$, the set of configurations that contribute dominantly to the thermal average in Eq. (**??**) $\mathcal{M}(\tilde{X}) = \{Y \mid V_{\mathrm{PT}}(Y, \tilde{X}) \leq \min_X V_{\mathrm{PT}}(X, \tilde{X}) + k_B T\}$, highlighted by blue boxes in Fig. **??**, will depend strongly on $\tilde{X}$. The average force $\mathcal{F}$ will then be subject to a sharp change as $\tilde{X}$ crosses a maximum of the sinusoidal potential, e.g. the one at $\tilde{X} = 0$.

We propose to estimate the influence of temperature by computing the derivative of the average force at a switching point, e.g. $\tilde{X} = 0$:

$$\partial \mathcal{F}/\partial \tilde{X}\Big|_{\tilde{X}=0} = -\partial^2 F/\partial \tilde{X}^2\Big|_{\tilde{X}=0} =: \chi. \tag{2.33}$$

For values of η large enough to sustain multiple minima and the possibility of stick-slip dynamics, as T decreases we expect this derivative to diverge as illustrated in Fig. **??**.

For convenience we introduce the rescaled $\tilde{x} = \tilde{X}/a$. By focusing on the low-temperature regime, we derive (Appendix **??**) an asymptotic expression for the partition function:

$$Z(\tilde{x}) \overset{\beta V_0 \to \infty}{\simeq} 2\frac{a}{\Lambda}\sqrt{\frac{\eta}{\eta+1}}\frac{e^{\beta V_0}}{\sqrt{2\pi\beta V_0}} \exp\left(-\frac{2\pi^2 \beta V_0}{\eta+1}(\tilde{x}^2 + 1/4)\right) \cosh\left(\frac{2\pi^2 \beta V_0 \tilde{x}}{\eta+1}\right). \tag{2.34}$$

While the exact partition function Eq. (**??**) is obviously periodic in $\tilde{X}$ with period a, the approximate expression Eq. (**??**) lacks any periodicity, and only holds in the range $-1/2 \leq \tilde{x} \leq 1/2$. The loss of periodicity is a result of the asymptotic expansion and we refer the curious reader to Appendix **??** for a detailed account.

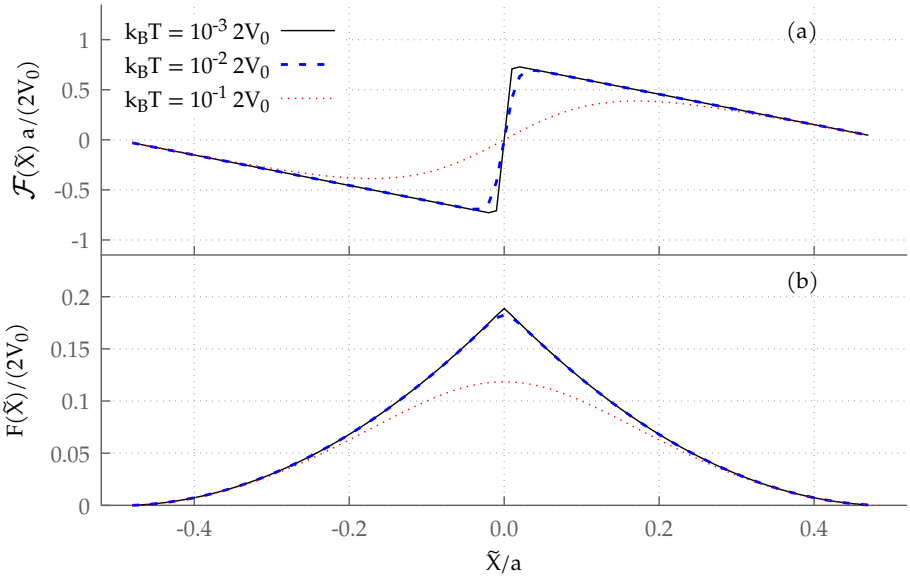

Figure 2.16: Panel (a): Average force Eq. (**??**) and panel (b): The free energy of the classical Prandtl-Tomlinson model, as a function of $\tilde{X}$ for $\eta = 12$.

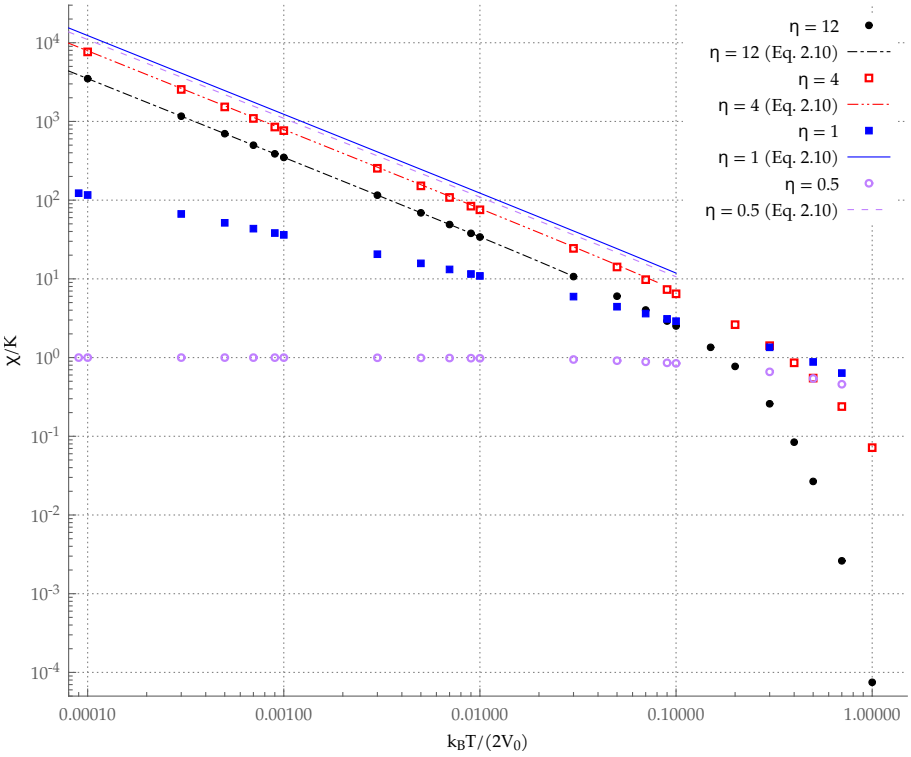

bsolute value of the e of the free energy of dtl-Tomlinson model ching point $\tilde{X} = 0$, as nperature. Curvature by numerical integra- lots) are compared to xpression Eq. (**??**) for sliding), 1 (transition and 12. Clearly, the ression Eq. (**??**) fails gime.

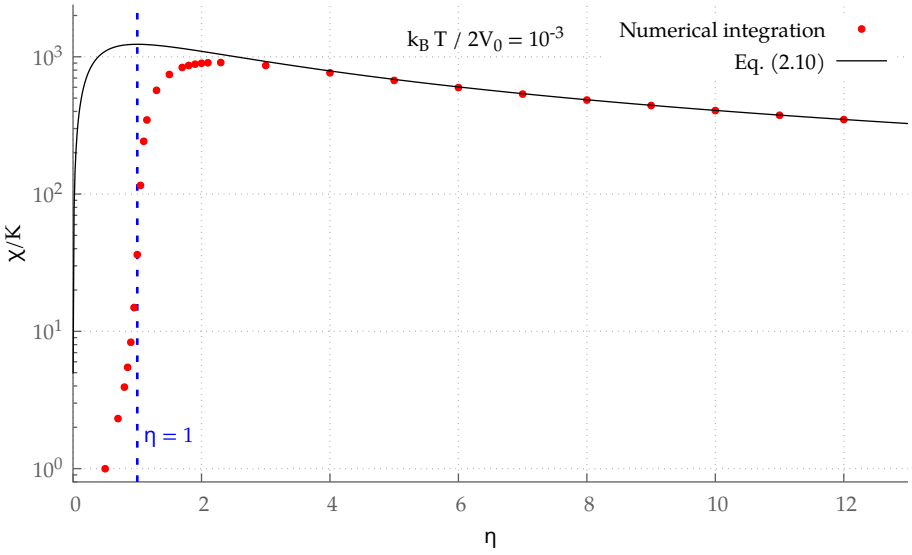

Figure 2.18: Absolute value of the second derivative of the free energy Eq. (**??**) at the switching point $\tilde{X} = 0$ as a function of η, for $k_B T/(2V_0) = 10^{-3}$.

We use Eq. (**??**) to calculate the free energy and its derivatives:

$$\begin{aligned} F(\tilde{x}) &= -\frac{1}{\beta}\log Z(\tilde{x}) \overset{\beta V_0 \to \infty}{\simeq} -V_0 + \frac{2\pi^2 V_0}{\eta+1}(\tilde{x}^2 + 1/4) - \frac{1}{\beta}\log\cosh\left(\frac{2\pi^2\beta V_0}{\eta+1}\tilde{x}\right) \\ \frac{\partial F(\tilde{x})}{\partial \tilde{x}} &= \frac{4\pi^2 V_0}{\eta+1}\tilde{x} - \frac{2\pi^2 V_0}{\eta+1}\tanh\left(\frac{2\pi^2\beta V_0}{\eta+1}\tilde{x}\right) \\ \frac{\partial^2 F(\tilde{x})}{\partial \tilde{x}^2} &= \frac{4\pi^2 V_0}{\eta+1} - 2\beta V_0 \frac{2\pi^2 V_0}{(\eta+1)^2}\operatorname{sech}^2\left(\frac{2\pi^2\beta V_0}{\eta+1}\tilde{x}\right). \end{aligned} \tag{2.35}$$

Focusing on the switching point $\tilde{x} = 0$, we note that the second derivative diverges as $\beta \propto T^{-1}$:

$$-\chi = \left.\frac{\partial^2 F(\tilde{x})}{\partial \tilde{x}^2}\right|_{\tilde{x}=0} = 2V_0\left[\frac{2\pi^2}{\eta+1} - 2V_0\beta\frac{\pi^2}{(\eta+1)^2}\right]. \tag{2.36}$$

Recalling Eq. (**??**), i.e. $2V_0/K = a^2\eta/(2\pi^2)$, we can rescale the previous expression to dimensionless quantities:

$$\frac{\chi}{K} = \left|\frac{\eta}{\eta+1} - \frac{1}{2}\frac{\eta}{(\eta+1)^2}2V_0\beta\right| = \left|\frac{\eta}{\eta+1} - \frac{1}{4\pi^2}\frac{\eta^2}{(\eta+1)^2}\beta K a^2\right| \tag{2.37}$$

In Fig. **??** we compare the outcome of Eq. (**??**) with the exact value of this quantity, obtained by means of the numerical integration of Eq. (**??**). Figure **??** reports the same comparison as a function of η for a fixed temperature. Note that the approximate asymptotic expression (**??**) agrees perfectly with the numerical result for $\eta \gtrsim 4$.

In this section we identified a promising necessary condition for stick-slip that can be linked to the equilibrium properties of the model. The presence of energy barriers between local minima, itself a necessary condition of stick-slip, is a sufficient condition for the sharp changes in the average force described above. Therefore we expect that there might be a lower bound on the absolute

value of the derivative of the average force, χ, below which no stick-slip can occur. A lower bound on χ then corresponds to an upper bound for T.

Although the resolution of Fig. **??** is lacking, direct comparison with Fig. **??** seems to indicate that this corresponds with the temperature range where χ decreases below the critical value $\chi_c \simeq K$.

Due to time constraints, we settle for this semi-quantitative result. We are confident that a more thorough analysis of this analogy between χ and the stick-slip phase diagram will quantitatively confirm the predictive power of our approach.

Chapter 3

The Quantum PT Model

Before considering any of the details of a fully quantum mechanical description of the Prandtl-Tomlinson system, we have to discuss the main features we expect to be able to study in order to characterize “stick-slip" motion. First of all, what would constitute stick-slip motion in a quantum mechanical setting? Suppose we substitute the Prandtl-Tomlinson particle with a wave function, how can we relate to the classical intuition behind stick-slip as the particle "being stuck" at a minimum and then suddenly "slipping forward"? In a strongly quantum regime we expect tunneling to invalidate this intuition: in such conditions the particle would be delocalized across multiple nearby minima and the notion of it being "stuck" in any of them is at best ill-defined, if not completely inapplicable. Similarly, any particle-related observable we may select to measure in order to establish the presence of stick-slip could be subject to a very similar critique as its observed average value will be influenced by the delocalization of the particle and, in this strongly quantum regime, will also be affected by close by minima. Although no inherently quantum mechanical quantity can describe stick-slip as we imagine it when we think about the classical Prandtl-Tomlinson system, we can still look for classical elements we wish to retain in our quantum mechanical model that would lend themselves to a similar interpretation. For example, the constant velocity motion of the slider is to be regarded as a necessarily classical phenomenon we would likely want to keep in the quantum model we are devising. This constant velocity motion could be described as an external condition fixed by the experimental setup, or explained by appealing to the general conceptual problem of the necessity of classical degrees of freedom (such as external fields) acting on any quantum mechanical system. Regardless, we can take advantage of this external parameter to look for observable quantities related to stick-slip motion that can be directly compared with their analog in the classical PT system.

In our discussion about the classical PT system we realized that a *necessary condition* for stick-slip motion is the presence of discontinuities (at $T = 0$) or sharp changes in the derivative of the free energy as a function of the position of the slider $\partial F(\tilde{X})/\partial \tilde{X}$ (see Fig. **??**). Presuming to be able to describe the low-velocity motion by studying equilibrium quantities, these sharp changes in the derivative describe the sharp variation in the force that the external experimenter has to apply on the slider to keep its velocity fixed when the “slip" occurs. In the classical model, before slip the experimenter would

need to pull the slider to the right to maintain its speed, while after slip one must suddenly brake to prevent the particle from pushing the slider forward. Such an abrupt change in the direction of the external force is precisely the discontinuity we observed and, most importantly, it does not depend on the precise mechanism by which “stick" or “slip" happen, but rather on the rapid change in the state of the particle. If any such a rapid change of state survives in the quantum mechanical case it could therefore be meaningfully studied by measuring the presence, or lack of, such discontinuities. Our choice to focus on equilibrium quantities is useful in preparation for the study of more complicated many-body models in which the static potential is substituted by e.g. an harmonic chain; in such a case the quantum dynamics is inaccessible to computer simulations, while equilibrium properties can be computed by imaginary-time Path Integral Monte Carlo (PIMC).

At a fixed position of the slider $\tilde{X}$, the quantum mechanical analog of the Prandtl-Tomlinson model consists of a 1D system governed by the Hamiltonian:

$$\hat{H}(\tilde{X}) = \frac{\hat{P}^2}{2M} + V_0 \cos\left(\frac{2\pi}{a}\hat{X}\right) + \frac{K}{2}(\hat{X} - \tilde{X})^2. \tag{3.1}$$

By introducing the oscillator frequency ω:

$$\omega = \sqrt{\frac{K}{M}}, \tag{3.2}$$

and the oscillator length l defined by:

$$\frac{\hbar^2}{2Ml^2} = \frac{Kl^2}{2} \implies l = \sqrt{\frac{\hbar}{M\omega}}, \tag{3.3}$$

we can recast the Hamiltonian Eq. (**??**) in the following form:

$$\hat{H}(\tilde{X}) = \underbrace{\frac{\hbar\omega}{2}\hat{p}^2}_{\hat{T}} + \underbrace{\frac{\hbar\omega}{2}(\hat{x} - \tilde{x})^2 + V_0 \cos\left(2\pi\frac{l}{a}\hat{x}\right)}_{\hat{V}(\hat{x},\tilde{x})}. \tag{3.4}$$

Here we introduced the rescaled dimensionless operators $\hat{p} = l\hat{P}/\hbar$, $\hat{x} = \hat{X}/l$ and $\tilde{x} = \tilde{X}/l$ as the *fixed* (dimensionless) slider position. By taking $\hbar\omega$ as unit of energy we can further rewrite Eq. (**??**) in a completely dimensionless form:

$$\hat{\mathfrak{h}}(\tilde{x}) := \frac{\hat{H}(\tilde{X})}{\hbar\omega} = \frac{1}{2}\left[\hat{p}^2 + (\hat{x} - \tilde{x})^2 + \frac{2V_0}{\hbar\omega}\cos\left(2\pi\frac{l}{a}\hat{x}\right)\right].$$

In this expression, the ratio $\hbar\omega/(Ka^2) = l^2/a^2$ measures the “quantumness" of the system through the ratio of the periodic potential corrugation to the oscillator quantum, which can alternatively be expressed in terms of the dimensionless length ratio l/a: $2V_0/(\hbar\omega) = 2\eta(Ka^2)/(4\pi^2)/(Kl^2) = \frac{\eta}{2\pi^2}(l/a)^{-2}$. In these terms the dimensionless Hamiltonian becomes:

$$\hat{\mathfrak{h}}(\tilde{x}) := \frac{\hat{H}(\tilde{X})}{\hbar\omega} = \frac{1}{2}\left[\hat{p}^2 + (\hat{x} - \tilde{x})^2 + \frac{\eta}{2\pi}\left(\frac{a}{l}\right)^2\cos\left(2\pi\frac{l}{a}\hat{x}\right)\right]. \tag{3.5}$$

We note here that the system’s behavior is determined by the following four dimensionless parameters:

- the classical Prandtl-Tomlinson parameter $\eta = 4\pi^2 V_0/(Ka^2)$ (introduced in Eq. (**??**) above);
- the "quantumness" ratio $\hbar\omega/(Ka^2) = (l/a)^2$;
- $\beta\hbar\omega$ that quantifies thermal occupation of the system's excited levels;
- the dimensionless position of the slider $\tilde{x} = \tilde{X}/l$.

We wish to study the equilibrium properties of this model and use it to establish a solid simulation procedure that can be extended to more computationally demanding many-body systems that cannot be directly diagonalized.

3.1 Exact diagonalization

The simplest approach to compute the equilibrium properties we are interested in is to directly diagonalize the Hamiltonian Eq. (**??**). In the canonical ensemble, having fixed the (dimensionless) position of the slider $\tilde{x}$, the partition function of the Prandtl-Tomlinson system is:

$$\begin{aligned} Z(\tilde{x}) &= \mathrm{Tr}\exp\left(-\beta\hat{H}(\tilde{x})\right) = \mathrm{Tr}\exp\left(-\beta\hbar\omega\hat{\mathfrak{h}}(\tilde{x})\right) = \\ &= \sum_{i=0}^{\infty} \mathrm{e}^{-\beta\hbar\omega e_i(\tilde{x})}, \end{aligned} \tag{3.6}$$

where $e_i(\tilde{x})$ is the i-th eigenvalue of $\hat{\mathfrak{h}}(\tilde{x})$. The exponential decrease of the terms in the series in Eq. (**??**) suggests to approximate the partition function by truncating the sum at index $I \in \mathbb{N}$, provided that $e_I(\tilde{x}) - e_0(\tilde{x}) \gg \frac{k_B T}{\hbar\omega}$:

$$Z(\tilde{x}) \approx \sum_{i=0}^{I} \mathrm{e}^{-\beta\hbar\omega e_i(\tilde{x})}, \quad F(\tilde{x}) = -\frac{1}{\beta}\log(Z(\tilde{x})). \tag{3.7}$$

We compute the eigenvalues by means of the shooting method, described in Appendix **??**, and report the resulting free energy surface in Figs. **??** and **??**.

As shown in Figs. **??** and **??**, there are two notable quantum mechanical effects: first of all the lowering of free energy barriers, and secondly a smoothing of the cusp at $\tilde{x} = 0$. Furthermore, both higher temperatures and higher "quantumness" regimes, measured by the ratio l^2/a^2, tend to smooth out the the first derivative of the free energy at $\tilde{x} = 0$, but in general in the quantum case no discontinuity occurs at $T = 0$, see Fig. **??**. As in the classical case, for $\eta < 1$ no discontinuity occurs either.

Ground-state energy

We can understand the behavior of the ground state energy close to $\tilde{X} = 0$ by appealing to a simple model inspired by tight-binding (TB) methods applied throughout chemistry and solid-state physics.

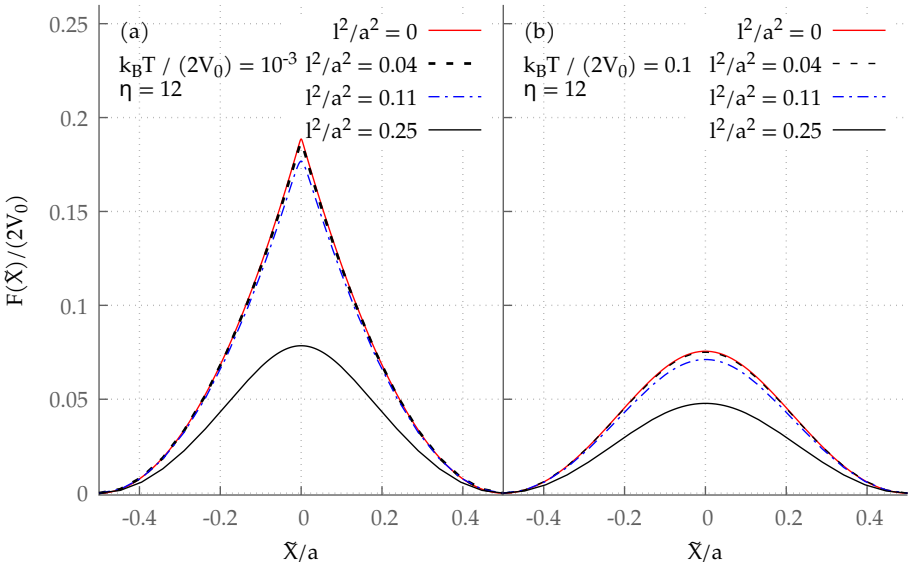

Figure 3.1: Comparison between the free energy of the classical model $F(\tilde{X})$ Eq. (**??**) (red, solid) and the free energy of the quantum system, Eq. (**??**). Panel (a): $k_BT = 0.001\,2V_0$, Panel (b): $k_BT = 0.1\,2V_0$. Different curves correspond to different regimes of quantumness: $l^2/a^2 = 0.04$ (black dashed line), $l^2/a^2 = 0.11$ (blue dot-dashed line), $l^2/a^2 = 0.25$ (black solid line). In the quantum evaluations, we approximate $F(\tilde{X})$ adopting the truncation of Eq. (**??**), with $I = 30$.

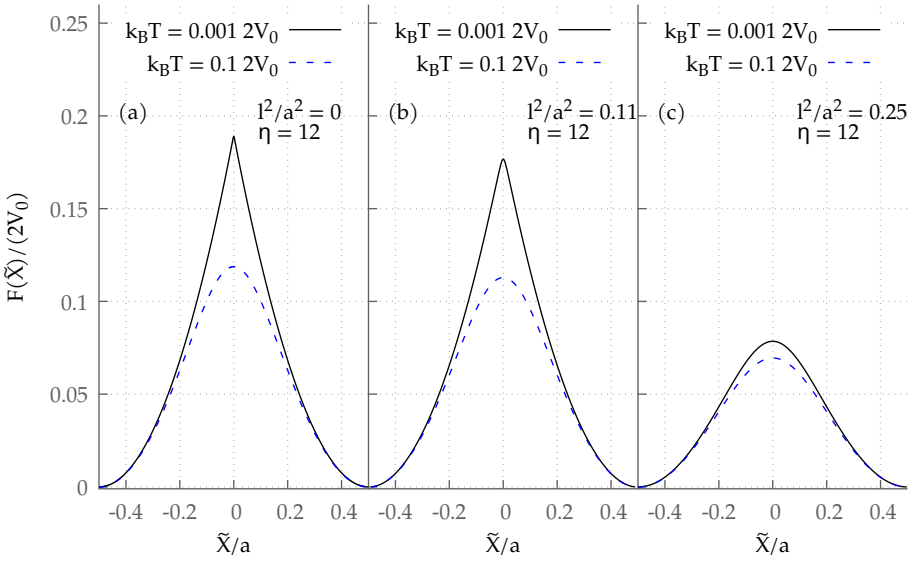

Figure 3.2: Comparison between the free energy $F(\tilde{X})$ of the classical PT model Eq. (**??**) (a), and the free energy of the quantum system Eq. (**??**) with $I = 30$ for $l^2/a^2 = 0.11$ (b), $l^2/a^2 = 0.25$ (c). Two temperatures are compared: a low one, namely $k_BT/(2V_0) = 10^{-3}$, and a very high one, namely $k_BT/(2V_0) = 10^{-1}$.

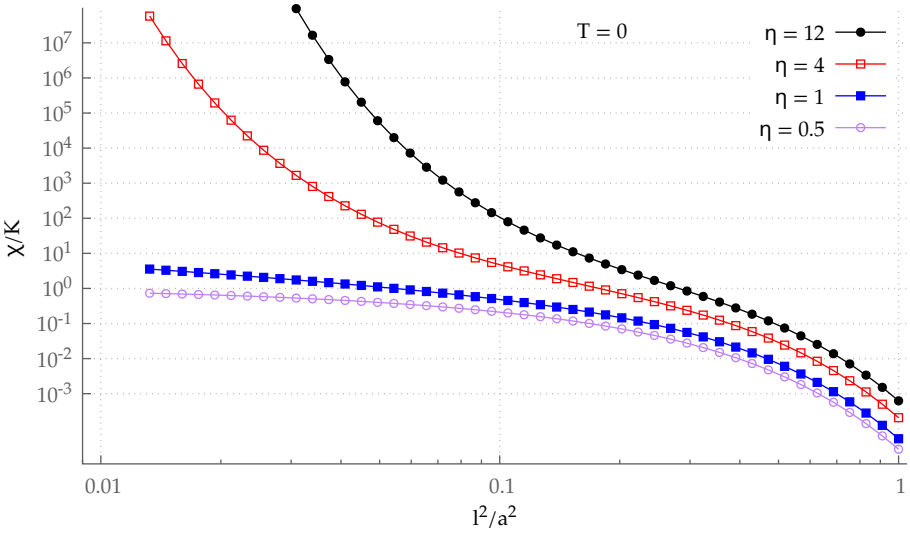

olute value of the sec-
f the ground-state en-
$\tilde{X})/\partial\tilde{X}^2|$ at the basin-
$\tilde{X} = 0$, for the $T = 0$
odel, as a function of
ss" $(l/a)^2$. For $\eta > 1$,
proaches the classical
), this second deriva-
onentially. The same
parameter as in Fig. **??**
e: $\eta = 12$ (black dots),
squares), $\eta = 1$ (blue
0.5 (purple circles).

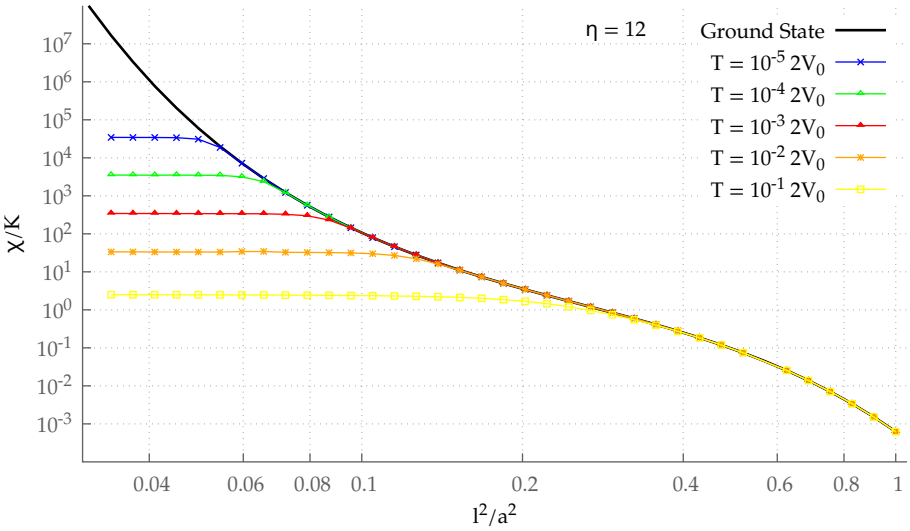

olute value of the sec-
f the free energy $\chi =$
the $\eta = 12$ quantum
asin-switching point
nction of the "quan-
and for a few temper-
e system approaches
the second derivative
ground-state value of
ck line). In the clas-
$^2 \to 0$, the second
ground-state energy
$_{=0}$ converges to a fi-
> 0, while for $T = 0$ it
an any power law of
s parameter $(l/a)^2$.

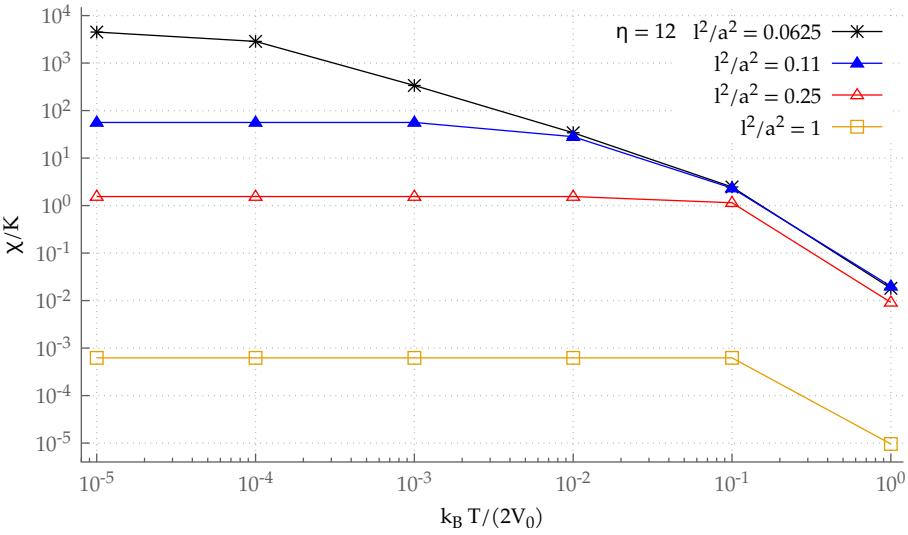

Figure 3.5: Absolute value of the second derivative of the free energy $\chi = |\partial^2 F(\tilde{X})/\partial \tilde{X}^2|$ at the basin-switching point $\tilde{X} = 0$ computed by means of exact diagonalization for the $\eta = 12$ quantum PT model, as a function of temperature $k_B T/(2V_0)$ and for a few values of "quantumness" $(l/a)^2$.

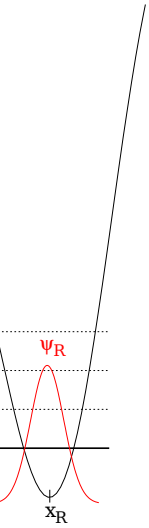

two energy levels
nding" description
ground state.

As depicted in Fig. **??**, for $\eta > 1$ the low-energy portion of the potential energy landscape resembles a double-well potential with two deep minima. These low-lying minima satisfy the equation:

$$\begin{aligned} \left.\frac{\partial V_{\mathrm{PT}}(X,\tilde{X})}{\partial X}\right|_{X=X_{\mathrm{L/R}}} &= 0, \\ K(X-\tilde{X}) - \frac{2\pi V_0}{a}\sin\left(\frac{2\pi}{a}X\right) &= 0. \end{aligned} \tag{3.8}$$

Now we restrict to the basin-switching point $\tilde{X} = 0$ and denote by the subscript L or R the quantities relative to the left and right well, respectively. Then the two minima will be symmetric: $X_{\mathrm{L}} = -X_{\mathrm{R}}$ and will lie close to the minima of the sinusoidal potential $\pm a/2$. Accordingly, to evaluate X_{R}, in Eq. (**??**) we expand $\sin(\cdot)$ around $a/2$. We obtain:

$$KX_{\mathrm{R}} + \frac{4\pi^2 V_0}{a^2}\left(X_{\mathrm{R}} - \frac{a}{2}\right) = 0 \implies X_{\mathrm{R}} = \frac{\eta}{\eta+1}\frac{a}{2}. \tag{3.9}$$

If we assume that for $\tilde{X}$ sufficiently close to 0 the position and shape of the minima remains constant, near the minima we can then approximate the potential with two harmonic wells with spring constant K_*:

$$\begin{aligned} K_* &= \left.\frac{\partial^2 V_{\mathrm{PT}}(X,\tilde{X}=0)}{\partial X^2}\right|_{X=X_{L/R}} = K - \frac{4\pi^2 V_0}{a^2}\cos\left(\frac{2\pi}{a}X_{L/R}\right) = \\ &= K\left[1+\eta\cos\left(\pi\frac{2\eta+1}{\eta+1}\right)\right] = K\,w(\eta)\,, \end{aligned}$$

where we introduce the spring-constant scaling factor

$$w(\eta) = 1 + \eta\cos\left(\pi\frac{2\eta+1}{\eta+1}\right) \tag{3.10}$$

and the associated vibrational length

$$l_* = \sqrt{\frac{\hbar}{\sqrt{MK_*}}} = l\,w(\eta)^{-1/4}\,. \tag{3.11}$$

We note in passing that $w(\eta) > 1$ for $\eta > 1$. This expansion around the two minima allows us to construct a two-level system spanned by the ground states of the two harmonic wells:

$$\psi_{L/R}(X) = \frac{\exp\left(-\frac{(X-X_{L/R})^2}{2l_*}\right)}{(\pi l_*^2)^{1/4}}. \tag{3.12}$$

The TB Hamiltonian matrix is:

$$\mathbf{H}^{\mathrm{TB}}(\tilde{X}) = \begin{bmatrix} \langle L|\hat{H}(\tilde{X})|L\rangle & \langle L|\hat{H}(\tilde{X})|R\rangle \\ \langle R|\hat{H}(\tilde{X})|L\rangle & \langle R|\hat{H}(\tilde{X})|R\rangle \end{bmatrix} = \begin{bmatrix} H_{\mathrm{LL}}(\tilde{X}) & H_{\mathrm{LR}}(\tilde{X}) \\ H_{\mathrm{RL}}(\tilde{X}) & H_{\mathrm{RR}}(\tilde{X}) \end{bmatrix}, \tag{3.13}$$

and the overlap matrix:

$$\mathbf{S}^{\mathrm{TB}} = \begin{bmatrix} 1 & \langle L|R\rangle \\ \langle R|L\rangle & 1 \end{bmatrix} = \begin{bmatrix} 1 & S_{\mathrm{LR}} \\ S_{\mathrm{RL}} & 1 \end{bmatrix}. \tag{3.14}$$

We note that having defined both ψ_L and ψ_R as real functions guarantees the symmetry of both the overlap and Hamiltonian matrices: $S_{\mathrm{LR}} = S_{\mathrm{RL}}$, $H_{\mathrm{LR}} = H_{\mathrm{RL}}$. The ground- and first-excited-state energies are obtained by solving the 2×2 generalized eigenvalue problem:

$$\mathbf{H}^{\mathrm{TB}}(\tilde{X})\psi^{\mathrm{TB}} = E^{\mathrm{TB}}\mathbf{S}^{\mathrm{TB}}\psi^{\mathrm{TB}}, \quad \psi^{\mathrm{TB}} \in \mathbb{R}^2\,. \tag{3.15}$$

The ground-state eigenvalue is:

$$\begin{aligned} E_0^{\mathrm{TB}}(\tilde{X}) = &\frac{H_{\mathrm{LL}} + H_{\mathrm{RR}} - 2S_{\mathrm{LR}}H_{\mathrm{LR}}}{2(1 - S_{\mathrm{LR}}^2)} \\ &- \frac{1}{2(1 - S_{\mathrm{LR}}^2)}\sqrt{(2S_{\mathrm{LR}}H_{\mathrm{LR}} - H_{\mathrm{LL}} - H_{\mathrm{RR}})^2 - 4(1 - S_{\mathrm{LR}}^2)(H_{\mathrm{LL}}H_{\mathrm{RR}} - H_{\mathrm{LR}}^2)} \end{aligned} \tag{3.16}$$

which we can rewrite as:

$$\begin{aligned} E_0^{\mathrm{TB}}(\tilde{X}) = &\frac{H_{\mathrm{LL}} + H_{\mathrm{RR}}}{2(1 - S_{\mathrm{LR}}^2)} - \frac{S_{\mathrm{LR}}H_{\mathrm{LR}}}{(1 - S_{\mathrm{LR}}^2)} \\ &- \frac{1}{(1 - S_{\mathrm{LR}}^2)}\sqrt{\left(\frac{H_{\mathrm{LL}} - H_{\mathrm{RR}}}{2}\right)^2 + H_{\mathrm{LR}}^2 - 2S_{\mathrm{LR}}H_{\mathrm{LR}}\left(\frac{H_{\mathrm{LL}} + H_{\mathrm{RR}}}{2}\right) + S_{\mathrm{LR}}^2 H_{\mathrm{LL}}H_{\mathrm{RR}}}. \end{aligned} \tag{3.17}$$

After a fair amount of Gaussian integrals we obtain the following expressions for the matrix elements and overlap integrals:

- The diagonal matrix elements read:

$$\begin{aligned} H_{\mathrm{LL}}(\tilde{X}) = &\frac{\hbar\omega_*}{4}\left\{1 + w(\eta)^{-1}\left[1 + 2\left(\frac{\mathrm{X_L} - \tilde{X}}{l_*}\right)^2\right]\right\} \\ &+ V_0 \exp\left(-\frac{\pi^2 l_*^2}{a^2}\right)\cos\left(\pi\frac{\eta}{\eta+1}\right) \\ H_{\mathrm{RR}}(\tilde{X}) = &\frac{\hbar\omega_*}{4}\left\{1 + w(\eta)^{-1}\left[1 + 2\left(\frac{\mathrm{X_R} - \tilde{X}}{l_*}\right)^2\right]\right\} \\ &+ V_0 \exp\left(-\frac{\pi^2 l_*^2}{a^2}\right)\cos\left(\pi\frac{\eta}{\eta+1}\right). \end{aligned} \tag{3.18}$$

- The off-diagonal matrix elements are:

$$\begin{aligned} H_{\mathrm{LR}}(\tilde{X}) = H_{\mathrm{RL}}(\tilde{X}) = &\\ = \exp\left(-\frac{X_{\mathrm{R}}^2}{l_*^2}\right)&\left\{\frac{\hbar\omega_*}{4}\left[1 - \frac{2X_{\mathrm{R}}^2}{l_*^2} + w(\eta)^{-1}\left(1 + \frac{2\tilde{X}^2}{l_*^2}\right)\right]\right. \\ &\left. + V_0 \exp\left(-\frac{\pi^2 l_*^2}{a^2}\right)\cos\left(\pi\frac{\eta}{\eta+1}\right)\right\}. \end{aligned} \tag{3.19}$$

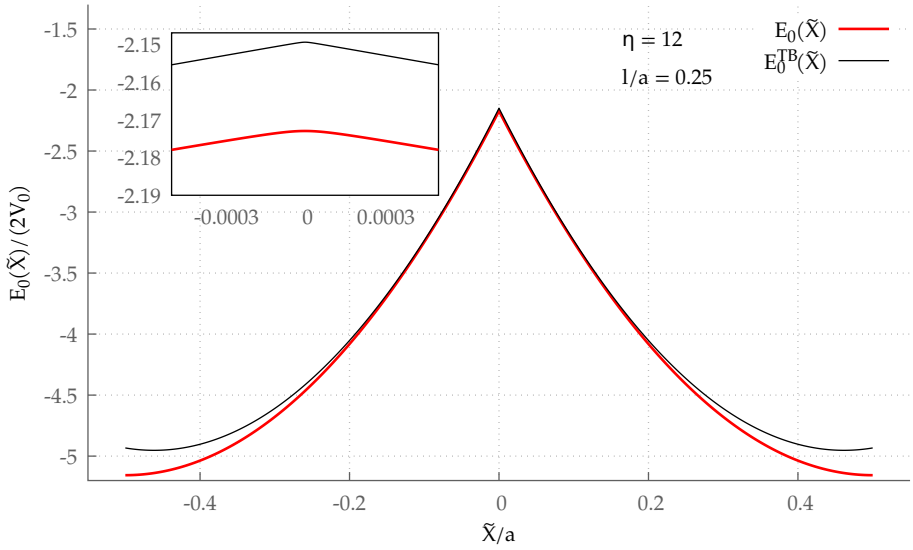

mparison between the ergy of the Quantum ated by means of the odel Eq. (**??**) and by zation, for $\eta = 12$,

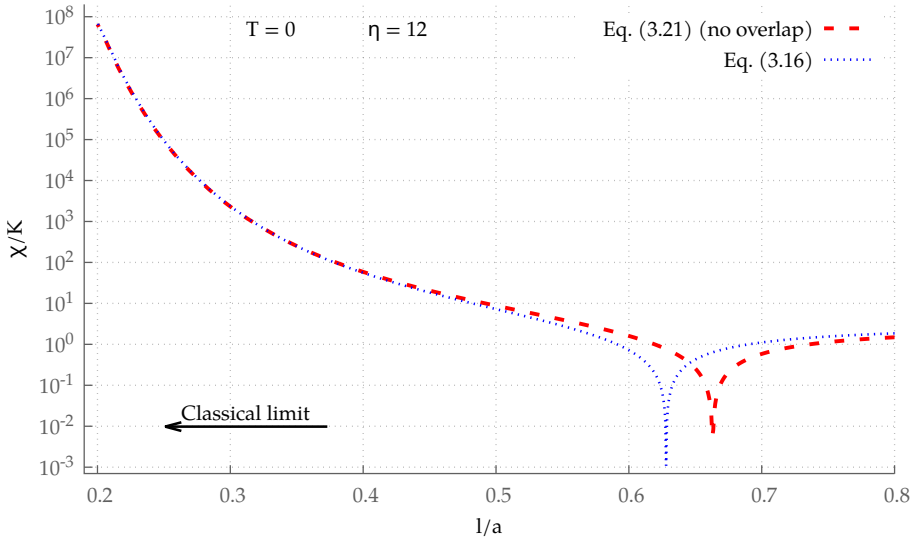

log plot of the second ground state energy PT model, $\partial^2 E_0^{TB}(\tilde{X} =$ tion of the "quantum- = 12. Two results are **?**) which includes the lue dot-dashed line) ch neglects them (red early, the behavior in t is not influenced by .

It is apparent that these tunneling energies decay exponentially when approaching the classical limit $(l/a)^2 \to 0$, or equivalently $(l_*/a)^2 \to 0$.

- The overlaps are:

$$S_{RL} = S_{LR} = \exp\left[-\left(\frac{X_L - X_R}{2l_*}\right)^2\right] = \exp\left[-\left(\frac{X_R}{l_*}\right)^2\right]. \tag{3.20}$$

They also vanish exponentially in the classical limit $(l/a)^2 \to 0$.

As reported in Fig. **??**, the TB energy of Eq. (**??**) approximates the ground-state energy fairly well in a region around $\tilde{X} = 0$.

As is clear from Fig. **??**, the overlaps S_{LR} play no role in the observed exponential behavior of $\partial^2 E_0^{TB}(\tilde{X} = 0)/\partial \tilde{X}^2$, so we will neglect them. This

approximation leads to a more tractable expression for the ground state energy:

$$E_0^{\mathrm{TB}}(\tilde{X}) = \frac{H_{\mathrm{LL}}(\tilde{X}) + H_{\mathrm{RR}}(\tilde{X})}{2} - \sqrt{\left(\frac{H_{\mathrm{LL}} - H_{\mathrm{RR}}}{2}\right)^2 + H_{\mathrm{LR}}^2}. \tag{3.21}$$

In order to extract information about the second derivative close to $\tilde{X} = 0$ we focus on the explicit dependence of each term on $\tilde{X}$:

$$\frac{H_{\mathrm{LL}} + H_{\mathrm{RR}}}{2} \sim C_1 + C_2\tilde{X}^2 \tag{3.22}$$

$$\left(\frac{H_{\mathrm{LL}} - H_{\mathrm{RR}}}{2}\right)^2 \sim C_3\tilde{X}^2 \tag{3.23}$$

$$H_{\mathrm{LR}}^2 \sim \exp\left(-2\frac{X_{\mathrm{R}}^2}{l_*^2}\right)\left(C_4 + C_5\tilde{X}^2 + O(\tilde{X}^4)\right). \tag{3.24}$$

Here we gather most terms into constants C_1, C_2, C_3, C_4, C_5 which do not influence the resulting singular behavior in the classical limit. If we now expand the square root in Eq. (**??**) we get:

$$\begin{aligned} E_0^{\mathrm{TB}}(\tilde{X}) &= C_1 + C_2\tilde{X}^2 - \exp\left(-\frac{X_{\mathrm{R}}^2}{l_*^2}\right)\sqrt{|C_4|}\sqrt{1 + \exp\left(2\frac{X_{\mathrm{R}}^2}{l_*^2}\right)\frac{C_3 + C_5}{C_4}\tilde{X}^2 + O(\tilde{X}^4)} = \\ &= C_1 + C_2\tilde{X}^2 - \exp\left(-\frac{X_{\mathrm{R}}^2}{l_*^2}\right)\sqrt{|C_4|}\left[1 + \exp\left(2\frac{X_{\mathrm{R}}^2}{l_*^2}\right)\frac{C_3 + C_5}{2C_4}\tilde{X}^2 + O(\tilde{X}^2)\right] \end{aligned} \tag{3.25}$$

Expanding $\sqrt{1+z\varepsilon} \overset{\varepsilon\to 0}{\sim} 1 + \frac{z}{2}\varepsilon$

This way, we can attribute the exponential growth of the second derivative for $(l/a)^2 \to 0$ to the exponential decrease of the tunneling matrix element H_{LR}. The full TB expression, valid for any quantumness is:

$$\frac{1}{K}\frac{\partial^2 E_0^{\mathrm{TB}}}{\partial\tilde{X}^2}\bigg|_{\tilde{X}=0, S_{\mathrm{LR}}=0} = 1 - \exp\left(\frac{\eta^2}{4(\eta+1)^2}\frac{a^2}{l_*^2}\right)\frac{\frac{a^2}{l^2}\left(\frac{\eta}{\eta+1}\right)^2 + \exp\left(-\frac{\eta^2}{2(\eta+1)^2}\frac{a^2}{l_*^2}\right)c}{|c|}, \tag{3.26}$$

where

$$c = \frac{\sqrt{w(\eta)}}{4}\left(1 - \frac{2X_{\mathrm{R}}^2}{l_*^2} + w^{-1}\right) + \frac{\eta}{4\pi^2}\frac{a^2}{l^2}\exp\left(-\pi^2\frac{l_*^2}{a^2}\right)\cos\left(\pi\frac{\eta}{\eta+1}\right). \tag{3.27}$$

As shown in Fig. **??**, the tight binding approach underestimates the tunneling matrix element H_{LR} and therefore overestimates $\partial^2 E_0(\tilde{X} = 0)/\partial\tilde{X}^2$. Nevertheless, the exponential behavior is correctly reproduced albeit with a different exponent, as is clear from Fig. **??**b.

Comparison of Fig. **??**a, Fig. **??** and Fig. **??** shows that both quantum and finite-temperature effects yield a smoother (free-)energy profile, but the approach to the $T = 0$ classical discontinuity in $\mathcal{F}$ is radically different. Qualitatively this suggests, as expected, that both tunneling and thermal effects will result in a preemption of stick-slip. Furthermore, we propose a quantitative comparison of Fig. **??** with the classical finite-temperature results Fig. **??** as a criterion to exclude stick-slip motion on the basis of the results of Sec. **??**.

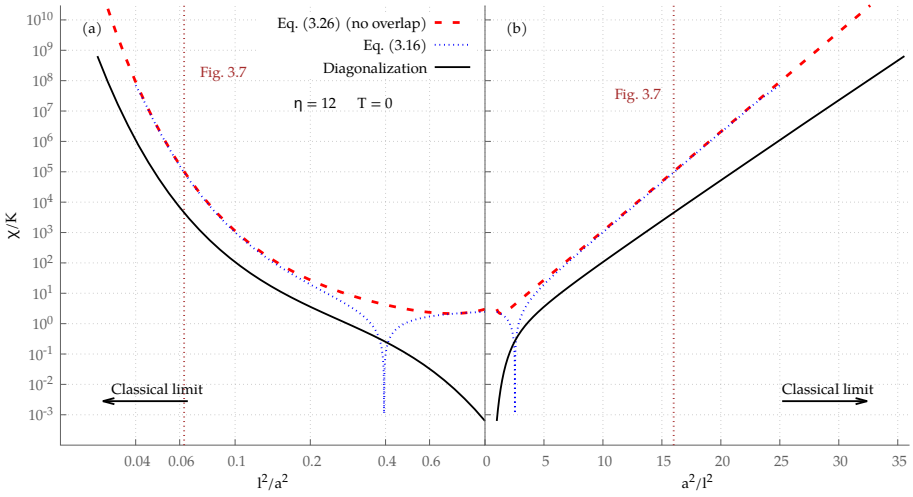

Figure 3.9: Comparison between the second derivative of the ground state energy of the Quantum PT model, $\partial^2 E_0(\tilde{X}=0)/\partial \tilde{X}^2$, for $\eta = 12$, calculated by exact diagonalization (solid black line) and with the TB model, both numerically calculating Eq. (**??**) (blue dot-dashed line), which includes the overlaps S_{LR}, and with the analytic result Eq. (**??**) (red dashed line) which neglects those overlaps. Panel (a): log-log plot as a function of the "quantumness" l^2/a^2. Panel (b): lin-log plot as a function of a^2/l^2 which shows that the exponential divergence in the classical limit is correctly captured by the TB model, except for an η-dependent constant in the exponent.

3.2 Imaginary-time path integral

As is well known, given a desired numerical precision the memory and time required to diagonalize a quantum Hamiltonian increases exponentially with its number of degrees of freedom, so the method presented in the previous section is impractical for many-body problems. A more computationally favorable and widely used approach to compute the equilibrium properties of many-body systems consists of imaginary-time Path-Integral Monte Carlo (PIMC) [**?**, **?**] simulations. This method exploits the similarity between the partition function of a quantum system in the path-integral formalism and that of a specific classical system, whose properties can be studied by well-established Markov-chain Monte-Carlo methods.

We develop here the tools necessary to understand PIMC, by applying it specifically to the Prandtl-Tomlinson model described in the previous section.[1] Given any operator $\hat{O}$, its average at equilibrium is given by:

y time" is due to
quantum time
librium Gibbs-

$$\xrightarrow{t=-i\beta\hbar} \exp\left(-\beta \hat{H}(\tilde{x})\right).$$

$$\left\langle \hat{O} \right\rangle_{\tilde{x}} = \mathrm{Tr}\, \hat{\varrho}(\tilde{x})\hat{O}, \quad \hat{\varrho}(\tilde{x}) = \frac{\mathrm{e}^{-\beta\hbar\omega\hat{\mathfrak{h}}(\tilde{x})}}{Z(\tilde{x})}. \tag{3.28}$$

PIMC calculations aim at computing these averages. The crucial difficulty here is the non-commutativity of the kinetic and potential energies, $\hat{T}$ and $\hat{V}$ defined in Eq. (**??**). Indeed, the exponential of the sum of two commuting operators A_1, A_2 is just the product of the individual exponentials:

$$\exp\left(\hat{A}_1 + \hat{A}_2\right) = \exp\left(\hat{A}_1\right)\exp\left(\hat{A}_2\right), \quad \text{if } \left[\hat{A}_1, \hat{A}_2\right] = 0. \tag{3.29}$$

In this case calculating averages, i.e. traces, is trivial: let $|a\rangle$ denote a basis of

common eigenstates of $\hat{A}_1$ and $\hat{A}_2$:

$$\hat{A}_1 |a\rangle = a_1 |a\rangle \, , \, \hat{A}_2 |a\rangle = a_2 |a\rangle \tag{3.30}$$

then:

$$\begin{aligned} \mathrm{Tr}\left\{\hat{O} \exp\left(\hat{A}_1 + \hat{A}_2\right)\right\} &= \sum_a \langle a|\hat{O} \exp\left(\hat{A}_1\right) \exp\left(\hat{A}_2\right)|a\rangle = \\ &= \sum_a \langle a|\hat{O}|a\rangle \exp(a_1 + a_2). \end{aligned} \tag{3.31}$$

However, in the case of Eq. (**??**) in general $\left[\hat{T}, \hat{V}\right] \neq 0$ and, while the equilibrium density matrix is still diagonal in the basis of eigenstates of $\hat{\mathfrak{h}}(\tilde{x})$, see Eq. (**??**), these cannot be easily computed. PIMC estimates equilibrium averages by approximating the matrix elements of $\hat{\varrho}(\tilde{x})$ in the (non-diagonal) x representation.

The first step toward PIMC is the Trotter splitting of operator exponentials:

$$\exp\left(-\beta \hat{H}(\tilde{x})\right) = \lim_{P\to\infty} \left(\exp\left(-\frac{\beta}{P}\hat{T}\right) \exp\left(-\frac{\beta}{P}\hat{V}(\hat{x}, \tilde{x})\right)\right)^P . \tag{3.32}$$

One way to understand why Eq. (**??**) is correct is to recall Baker-Campbell-Hausdorff's formula [**?**, **?**]:

$$\mathrm{e}^{\hat{O}}\mathrm{e}^{\hat{O}'} = \exp\left(\hat{O} + \hat{O}' + \frac{1}{2}\left[\hat{O}, \hat{O}'\right] + \frac{1}{12}\left[\hat{O}, \left[\hat{O}, \hat{O}'\right]\right] + \dots\right), \tag{3.33}$$

with

$$\hat{O} = \frac{\beta}{P}\hat{T}, \quad \hat{O}' = \frac{\beta}{P}\hat{V}(\hat{x}, \tilde{x}). \tag{3.34}$$

We can then raise Eq. (**??**) to the power of P:

$$\left(\mathrm{e}^{\hat{O}}\mathrm{e}^{\hat{O}'}\right)^P = \exp\left[P\left(\hat{O} + \hat{O}' + \frac{1}{2}\left[\hat{O}, \hat{O}'\right] + \frac{1}{12}\left[\hat{O}, \left[\hat{O}, \hat{O}'\right]\right] + \dots\right)\right], \tag{3.35}$$

and note that all terms in the exponent except $\hat{O} + \hat{O}'$ are $o(P^{-1})$. From the expression of the next-to-leading term in Eq. (**??**):

$$\exp\left(\frac{P}{2}\left[\frac{\beta}{P}\hat{T}, \frac{\beta}{P}V(\hat{x}, \tilde{x})\right]\right) = \exp\left\{-\frac{1}{2P}\left(\frac{\beta\hbar\omega}{2}\right)^2 \left[\hat{p}^2, (\hat{x} - \tilde{x})^2 + \frac{2V_0}{\hbar\omega}\cos\left(2\pi\frac{l}{a}\hat{x}\right)\right]\right\} \tag{3.36}$$

we note that the Trotterization (i.e. the splitting of the exponential) is effective as long as:

$$\frac{1}{2P}\left(\frac{\beta\hbar\omega}{2}\right)^2 \ll 1 \iff P \gg P_{\min} = \left\lceil \frac{(\beta\hbar\omega)^2}{8} \right\rceil . \tag{3.37}$$

In particular, by rewriting:

$$\beta\hbar\omega = \beta K a^2 \frac{l^2}{a^2} \tag{3.38}$$

we note that, for any fixed (inverse) temperature β and spring constant K, the effective number of Trotter slices needed to correctly capture the quantum behaviour $P_{\min}$, Eq. (**??**), grows as l^4/a^4.

We can use Eq. (**??**) to evaluate the partition function, Eq. (**??**):

$$\begin{aligned} Z(\tilde{x}) &= \mathrm{Tr}\exp\Big(-\beta\hat{H}(\tilde{x})\Big) = \int \mathrm{d}x\,\langle x|\exp\Big(-\beta\hat{H}(\tilde{x})\Big)|x\rangle = \\ &= \lim_{P\to\infty}\int \mathrm{d}x\,\langle x|\left[\exp\left(-\frac{\beta}{P}\hat{T}\right)\exp\left(-\frac{\beta}{P}\hat{V}(\hat{x},\tilde{x})\right)\right]^P|x\rangle\,. \end{aligned} \tag{3.39}$$

We need to calculate the following off-diagonal matrix elements:

$$\varrho_{\mathrm{split}}(y,w) = \left\langle y\middle|\exp\left(-\frac{\beta}{P}\hat{T}\right)\exp\left(-\frac{\beta}{P}\hat{V}(\hat{x},\tilde{x})\right)\middle|w\right\rangle, \tag{3.40}$$

because we can then rewrite Eq. (**??**) in terms of ϱ_{split} by explicitly writing the split exponentials in terms of their (dimensionless) integral kernels:[2]

n think of this as

$= \mathbb{1}$,

ntials.

$$\begin{aligned} Z(\tilde{x}) &= \int \mathrm{d}x\,\langle x|\exp\Big(-\beta\hbar\omega\hat{\mathfrak{h}}(\tilde{x})\Big)|x\rangle = \\ &= \lim_{P\to\infty}\int \mathrm{d}x\,\langle x|\left[\exp\left(-\frac{\beta}{P}\frac{\hbar\omega}{2}\hat{p}^2\right)\exp\left(-\frac{\beta}{P}\hat{V}(\hat{x},\tilde{x})\right)\right]^P|x\rangle = \\ &= \lim_{P\to\infty}\int \mathrm{d}x\int\left(\prod_{i=1}^{P-1}\mathrm{d}x_i\right)\varrho_{\mathrm{split}}(x,x_1)\varrho_{\mathrm{split}}(x_1,x_2)\ldots\varrho_{\mathrm{split}}(x_{P-1},x). \end{aligned} \tag{3.41}$$

The evaluation of $\varrho_{\mathrm{split}}(y,w)$ goes as follows:

$$\begin{aligned} \varrho_{\mathrm{split}}(y,w) &= \left\langle y\middle|\exp\left(\frac{\beta\hbar\omega}{2P}\hat{p}^2\right)\exp\left(\frac{\beta}{P}\hat{V}(\hat{x},\tilde{x})\right)\middle|w\right\rangle = \\ &= \exp\left(\frac{\beta}{P}V(w,\tilde{x})\right)\left\langle y\middle|\exp\left(-\frac{\beta\hbar\omega}{2P}(\hat{p})^2\right)\middle|w\right\rangle = \\ &= \exp\left(-\frac{\beta}{P}V(w,\tilde{x})\right)\int_{-\infty}^{\infty}\frac{\mathrm{d}k'}{2\pi}\exp\left(-\frac{\beta\hbar\omega}{2P}k'^2\right)\exp\big(ik'(w-y)\big) = \\ &= \exp\left(-\frac{\beta}{P}V(w,\tilde{x})\right)\sqrt{\frac{P}{2\pi\beta\hbar\omega}}\exp\left(-\frac{P}{2\beta\hbar\omega}(w-y)^2\right), \end{aligned} \tag{3.42}$$

where the last equality results from standard Gaussian integration:

$$\int_{-\infty}^{+\infty}\mathrm{d}x\,\mathrm{e}^{-Ax^2+xB} = \sqrt{\frac{\pi}{A}}\,\mathrm{e}^{B^2/(4A)}\,. \tag{3.43}$$

If we denote $\mathbf{x} = (x_1, \ldots, x_P)$ and $x_{P+1} = x_1$, we can rewrite Eq. (**??**):

$$Z(\tilde{x}) = \lim_{P\to\infty} \left(\frac{P}{2\pi\beta\hbar\omega}\right)^{P/2} \int_{\substack{\mathbb{R}^P \\ x_{P+1}=x_1}} \mathrm{d}\mathbf{x} \exp\left(-\frac{P^2}{\beta\hbar\omega} \overbrace{\frac{1}{P}\sum_{p=1}^{P} \frac{1}{2}(x_{p+1}-x_p)^2}^{E_K(\mathbf{x})} \right) \tag{3.44}$$

$$\exp\left(\underbrace{-\frac{\beta\hbar\omega}{2} \frac{1}{P}\sum_{p=1}^{P} \left[\overbrace{(x_p-\tilde{x})^2 + \frac{2V_0}{\hbar\omega}\cos\left(2\pi\frac{l}{a}x_p\right)}^{\tilde{V}(x_p;\tilde{x})} \right]}_{U_{\mathrm{PT}}(\mathbf{x};\tilde{x})} \right).$$

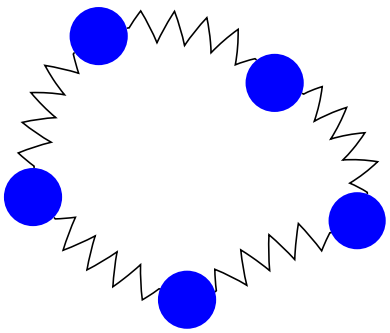

Figure 3.10: Cartoon of the classical polymer whose partition function is described by the integral in Eq. (**??**), for $P = 5$. The limit $P \to \infty$ yields the quantum partition function.

Before discussing the role of the newly-defined quantities E_K and U_{PT}, we highlight the correspondence between $Z(\tilde{x})$, Eq. (**??**), and the $P \to \infty$ limit of the partition function of a classical polymer of P beads, see Fig. **??**, such that:

- The first and last bead (indexes $p = 1$ and $p = P + 1$) coincide;
- The p-th bead is connected by springs of stiffness

$$K_P = \frac{P}{\beta\hbar\omega}, \tag{3.45}$$

  to the $(p-1)$-th and $(p+1)$-th (with periodic boundary conditions);
- Each bead experiences the classical PT potential V_{PT} reduced by a factor of P.

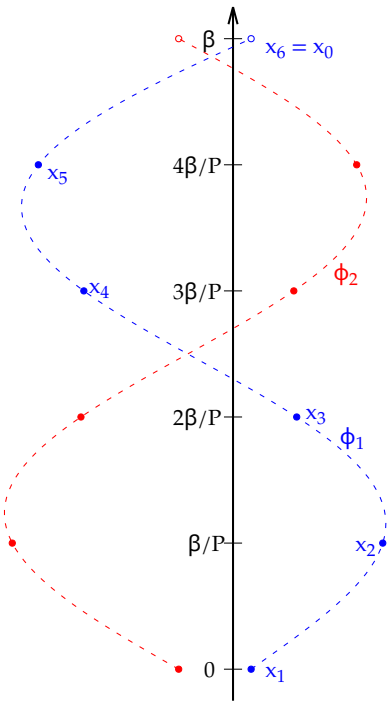

Figure 3.11: Cartoon of the discretization of two periodic paths ϕ_1, ϕ_2, for $P = 5$.

This point of view clarifies that we can calculate equilibrium averages of quantum observables as the $P \to \infty$ limit of equilibrium averages of corresponding observables for the polymer we just described. In the following we will refer to the intermediate variables x_p as "Trotter slices" or "imaginary-time slices", a term that clarifies their origin as different copies of the system at different imaginary times $(p-1)\beta/P$.

Alternatively, we can interpret the Trotterization procedure as a specific algorithm to weight all of the possible periodic paths in imaginary time $\phi : [0, \beta] \to \mathbb{R}$, $\phi(0) = \phi(\beta)$. Indeed we can picture the position x_p of the p-pth bead in the polymer as the image of the point $(p-1)\beta/P$ under ϕ, see Fig. **??**. Calculating the P-dimensional integral in Eq. (**??**) corresponds to averaging over all possible functions ϕ weighted depending on their values at the discrete points $(p-1)\beta/P$. In this analogy, the limit $P \to \infty$ is the continuum limit for the discrete representation of the path ϕ. This mental model of the Trotterization procedure is the rationale for the name *Path Integral* Monte Carlo.

In Eq. (**??**) we introduced a few important quantities: the total elastic energy E_K of the imaginary-time springs, the total potential energy $U_{\mathrm{PT}}(\mathbf{x}, \tilde{x})$

and the potential energy contributions $\tilde{V}(x;\tilde{x})$ of each Trotter slice. With this formalism, we can compute the average value $\left\langle \hat{O} \right\rangle_{\tilde{x}}$ of an operator function of the position operator, $\hat{O} = O(\hat{x})$, according to Eqs. (**??**) and (**??**):

$$\begin{aligned} \left\langle \hat{O} \right\rangle_{\tilde{x}} &= \mathrm{Tr}\left(\hat{\varrho}(\tilde{x})O(\hat{x})\right) = \mathrm{Tr}\left(\frac{\exp\left(-\beta\hbar\omega\hat{\mathfrak{h}}(\tilde{x})\right)}{Z(\tilde{x})}O(\hat{x})\right) = \\ &= \lim_{P\to\infty}\left(\frac{P}{2\pi\beta\hbar\omega}\right)^{P/2}\int_{\mathbb{R}^P}\mathrm{d}\mathbf{x}\, O(x_1)\frac{\exp\left[-\frac{P^2}{\beta\hbar\omega}E_K(\mathbf{x}) - \frac{\beta\hbar\omega}{2}U_{\mathrm{PT}}(\mathbf{x},\tilde{x})\right]}{Z(\tilde{x})}. \end{aligned} \tag{3.46}$$

More general operators or thermodynamic quantities of interest can be approximated in a similar manner, albeit requiring more involved calculations to lead to an expression that can be cast in the form of Eq. (**??**).

Metropolis-Hastings algorithm

The computation of highly dimensional integrals, like Eq. (**??**), is most easily carried out using Markov Chain Monte Carlo methods, which rely on a stochastic process to explore the integral's domain, i.e. the polymer's configuration space. We focus here on the Metropolis-Hastings algorithm [**?**] (MHA) which consists of a specific way to explore the configuration space by updating the state of the system $\mathbf{x} = (x_1, \ldots, x_P)$ according to a transition rule:

$$\mathcal{T}(\mathbf{x}' \leftarrow \mathbf{x}), \tag{3.47}$$

chosen so that the equilibrium distribution of the Markov process coincides with the distribution we wish to sample. In the case of PIMC we will sample the Boltzmann distribution of the classical polymer:

$$P_P(\mathbf{x};\tilde{x}) = \left(\frac{P}{2\pi\beta\hbar\omega}\right)^{P/2}\frac{\exp\left[-\frac{P^2}{\beta\hbar\omega}E_K(\mathbf{x}) - \frac{\beta\hbar\omega}{2}U_{\mathrm{PT}}(\mathbf{x},\tilde{x})\right]}{Z(\tilde{x})}. \tag{3.48}$$

To guarantee the convergence to the desired probability distribution two properties are sufficient: *ergodicity* and a transition rule that satisfies the *detailed balance* condition. The chain is said to be ergodic if any state of the system may be reached in a finite number of transitions. This speaks of the ability of the process to fairly explore the whole state space, a crucial property to ensure correct sampling. If the chain is ergodic then choosing a transition rule that satisfies the detailed balance condition:

$$P_P(\mathbf{x};\tilde{x})\mathcal{T}(\mathbf{x}' \leftarrow \mathbf{x}) = P_P(\mathbf{x}';\tilde{x})\mathcal{T}(\mathbf{x} \leftarrow \mathbf{x}'), \tag{3.49}$$

is sufficient to guarantee the match between the equilibrium distribution and P_P.

In order to guarantee detailed balance, the MHA algorithm splits the transition in two steps:

$$\mathcal{T}(\mathbf{x}' \leftarrow \mathbf{x}) = \mathcal{P}(\mathbf{x}' \leftarrow \mathbf{x})\mathcal{A}(\mathbf{x}' \leftarrow \mathbf{x}), \tag{3.50}$$

where $\mathcal{P}(\mathbf{x}' \leftarrow \mathbf{x})$ is referred to as the proposal distribution and

$$\mathcal{A}(\mathbf{x}' \leftarrow \mathbf{x}) = \min\left[1, \frac{\mathcal{P}(\mathbf{x} \leftarrow \mathbf{x}')P_P(\mathbf{x}')}{\mathcal{P}(\mathbf{x}' \leftarrow \mathbf{x})P_P(\mathbf{x})}\right], \tag{3.51}$$

is the acceptance probability. Practically speaking, one generates a new configuration $\mathbf{x}'$ by sampling from $\mathcal{P}(\mathbf{x}' \leftarrow \mathbf{x})$ and then accepts it with probability $\mathcal{A}(\mathbf{x}' \leftarrow \mathbf{x})$. The proposed configurations are usually referred to as "moves". After a rejected move the system will remain in the same state until the next accepted transition.

An integral like Eq. (**??**) can be estimated by first generating a Monte Carlo sequence of J configurations $\mathbf{x}_j = (x_{1j}, \ldots, x_{Pj})$ with the MHA algorithm and then averaging over these configurations:

$$\left\langle \hat{O} \right\rangle_{\tilde{x}} \approx \bar{O} = \frac{1}{J}\sum_{j=1}^{J} O(x_{1j}) = \frac{1}{J}\sum_{j=1}^{J} O_j = \left\langle O_j \right\rangle. \tag{3.52}$$

The standard error of the estimate $\bar{O}$ is:

$$\sigma_O = \sqrt{\frac{\kappa_O \nu_O}{J}}, \tag{3.53}$$

where

$$\nu_O = \left\langle (O_j - \bar{O})^2 \right\rangle \tag{3.54}$$

is the variance of the time series O_j and

$$\kappa_O = 1 + 2\sum_{k=1}^{\infty} \frac{\left\langle (O_k - \bar{O})(O_0 - \bar{O}) \right\rangle}{\nu_O} \tag{3.55}$$

is the (integrated) *correlation time*. κ_O measures the average number of steps necessary to decorrelate O_j, that is to say J/κ_O is the effective number of independent measurements of O. κ_O is strongly dependent on the measured quantity, the proposed moves and the physical system. As is clear from Eq. (**??**), the shorter the correlation time the more efficient the chain is. To ensure the correct estimation of statistical errors we calculate κ_O using the algorithm described in [**?**] and implement[**?**] data blocking [**?**].

Metadynamics

A well known difficulty of the MHA algorithm is that low-temperature sampling of the distribution in Eq. (**??**) may fail to be ergodic if the barriers between competing local minima are very high compared to thermal energy β^{-1}. This is a quite concrete possibility for the PT model at hand, which relies precisely on the crossing of energy barriers. Therefore, in order to work around this problem, we implement[**?**] metadynamics [**?**], a method that proved itself useful for enhancing the exploration of complex Free Energy Surfaces (FES) of classical systems. Metadynamics enhances the probability of sampling configurations with low Boltzmann weights by regularly modifying the free energy of the system. First of all one selects a small set of collective variables

(CVs) $\mathbf{S} = (S_1, \ldots, S_d)$, i.e. functions of the "microscopic" degrees of freedom of the system that describe important properties suitable to discriminate between local free-energy minima, and then computes $F(\mathbf{S})$ by performing a non-Markovian random walk in configuration space.

For our quantum Prandtl-Tomlinson model we select the following two CVs:

- E_K: the average energy of the springs connecting particles in imaginary time, see Eq. (**??**). This quantity is related to the quantum kinetic energy by:
$$\beta \left\langle \hat{T} \right\rangle = \frac{P}{2} - P^2 \left\langle E_K \right\rangle , \tag{3.56}$$
and should allow the exploration of tunneling and delocalization effects on the resulting free energy;
- x: the position of one of the particles in the chain, say x_1. This CV should be able to differentiate between local minima in the potential energy, and acts as a useful variable to compare the free energy of the classical system to the one computed through metadynamics, as will be clear in the following.

We now rewrite the integrand of Eq. (**??**) as an explicit function of the CVs:

$$\begin{aligned} Z(\tilde{x}) &= \lim_{P\to\infty} P^{P/2} \int_{\mathbb{R}^P} \frac{\mathrm{d}\mathbf{x}}{(2\pi\beta\hbar\omega)^{P/2}} \exp\left(-\frac{P^2}{\beta\hbar\omega} E_K(\mathbf{x}) - \frac{\beta\hbar\omega}{2} U_{\mathrm{PT}}(\mathbf{x};\tilde{x})\right) = \\ &= \lim_{P\to\infty} P^{P/2} \int_{\mathbb{R}^P} \frac{\mathrm{d}\mathbf{x}}{(2\pi\beta\hbar\omega)^{P/2}} \int_{-\infty}^{\infty} \mathrm{d}E_K \delta(E_K - E_K(\mathbf{x})) \\ &\qquad\qquad \exp\left(-\frac{P^2}{\beta\hbar\omega} E_K - \frac{\beta\hbar\omega}{2} U_{\mathrm{PT}}(\mathbf{x};\tilde{x})\right) = \\ &= \lim_{P\to\infty} \int_{\mathbb{R}} \mathrm{d}E_K \int_{\mathbb{R}} \mathrm{d}x\, g_P(x, E_K) \exp\left(-\frac{P^2}{\beta\hbar\omega} E_K - \frac{\beta\hbar\omega}{2} \frac{1}{P} \tilde{V}(x;\tilde{x})\right) \end{aligned} \tag{3.57}$$

where

$$\begin{aligned} g_P(x, E_K) = \frac{P^{P/2}}{\sqrt{2\pi\beta\hbar\omega}} \int_{\mathbb{R}^{P-1}} \left(\prod_{p=2}^{P} \frac{\mathrm{d}x_p}{\sqrt{2\pi\beta\hbar\omega}}\right) \delta(E_K - E_K(x, x_2, \ldots, x_p)) \\ \exp\left(-\frac{\beta\hbar\omega}{2} \frac{1}{P} \sum_{p=2}^{P} \tilde{V}(x_p;\tilde{x})\right), \end{aligned} \tag{3.58}$$

is the density of states of the polymer at given total (dimensionless) elastic energy $E_K(\mathbf{x}) = E_K$ and position of one of the particles $X_1 = lx_1 = lx = X$. We can therefore rewrite the partition function, Eq. (**??**), as the integration of a reduced partition function $Z_P(x, E_K; \tilde{x})$:

$$\begin{aligned} Z(\tilde{x}) &= \lim_{P\to\infty} \int \mathrm{d}E_K \mathrm{d}x Z_P(x, E_K; \tilde{x}), \\ &= \lim_{P\to\infty} \int_{\mathbb{R}} \mathrm{d}E_K \int_{\mathbb{R}} \mathrm{d}x \exp\big(-\beta F_P(x, E_K; \tilde{x})\big) \end{aligned} \tag{3.59}$$

given by

$$Z_P(x, E_K; \tilde{x}) = g_P(x, E_K; \tilde{x}) \exp\left(-\frac{P^2}{\beta\hbar\omega} E_K - \frac{\beta\hbar\omega}{P} \tilde{V}(x; \tilde{x})\right). \tag{3.60}$$

As usual we can define the associated free energy:

$$F_P(x, E_K; \tilde{x}) = -\frac{1}{\beta} \log(Z_P(x, E_K; \tilde{x})).$$

Metadynamics can be used to calculate $F_P(x, E_K; \tilde{x})$ by adding a simulation-time-dependent repulsive bias potential $V_{\text{meta}}(\mathbf{S}, t_{\text{MC}})$ to the energy and performing a Metropolis walk in configuration space. The repulsive potential has the goal of pushing the system away from metastable minima by gradually increasing the free energy of frequently visited regions of CV space. This is achieved by adding to V_{meta} a repulsive kernel localized close to the instantaneous value of the CVs, $\mathbf{S}(t_{\text{MC}})$, every τ_G timesteps during the simulation:

$$V_{\text{meta}}(\mathbf{S}, t_{\text{MC}}) = \sum_{n \in \mathbb{N}: n\tau_G < t_{\text{MC}}} w \exp\left(-\sum_{i=1}^{d} \frac{(S_i - S_i(n\tau_G))^2}{2\sigma_i^2}\right). \tag{3.61}$$

The established practice for metadynamics is to take a Gaussian centered around $\mathbf{S}(t_{\text{MC}})$ as repulsive kernel. The height w of the Gaussian influences the "filling speed", and the variances σ_i^2 influence the resolution of the reconstructed FES. This bias will force the system away from frequently visited configurations, which correspond to low-free-energy states, effectively filling the FES and approximating it up to a constant:

$$\lim_{t_{\text{MC}} \to \infty} V_{\text{meta}}(\mathbf{S}, t_{\text{MC}}) \approx -F(\mathbf{S}) + C. \tag{3.62}$$

In fact, metadynamics suffers from convergence problems that encouraged its refinement. We therefore implement[**?**] Well-Tempered Metadynamics [**?**]: during the simulation the bias potential height w is changed according to the following procedure:

$$w(t_{\text{MC}}) = w \exp\left(-\frac{V_{\text{wtm}}(\mathbf{S}(t_{\text{MC}}), n\tau_G)}{k_{\text{B}}\Delta T}\right), \qquad n = \left\lfloor \frac{t_{\text{MC}}}{\tau_G} \right\rfloor. \tag{3.63}$$

The size of the Gaussians decreases in the most visited regions of CV space, guaranteeing convergence of the method [**?**]. The new parameter ΔT can be interpreted as the maximum height of any free-energy barrier the well-tempered metadynamics simulation will be able to overcome effectively. In this scheme, similarly to Eq. (**??**), the bias potential is computed as:

$$V_{\text{wtm}}(\mathbf{S}, t_{\text{MC}}) = \sum_{n \in \mathbb{N}: n\tau_G < t_{\text{MC}}} w(t_{\text{MC}}) \exp\left(-\sum_{i} \frac{(S_i - S_i(n\tau_G))^2}{2\sigma_i^2}\right). \tag{3.64}$$

The decrease in the height of Gaussians reduces the fluctuations plaguing metadynamics and ensures the long-time convergence to the FES:

$$\beta F(\mathbf{S}) = \lim_{t_{\text{MC}} \to \infty} -\frac{\gamma_{\text{wtm}}}{k_{\text{B}}\Delta T} V_{\text{wtm}}(\mathbf{S}, t_{\text{MC}}) + C, \tag{3.65}$$

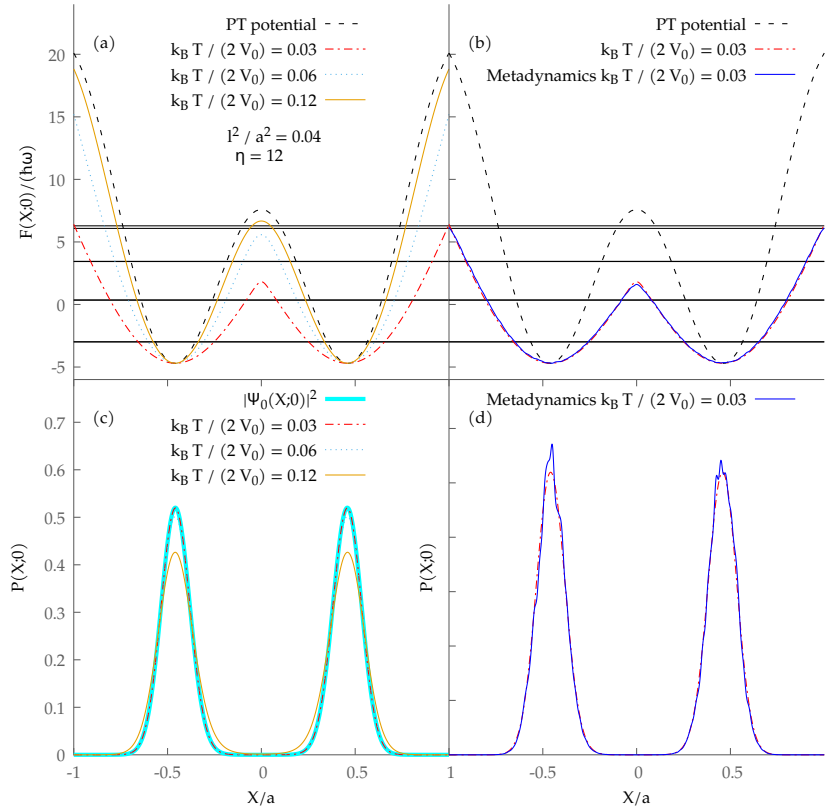

Figure 3.12: (a) Comparison between the classical PT potential $V_{\mathrm{PT}}(x;\tilde{x}=0)$ and the constrained free energy $F(x;\tilde{x}=0) = -\beta^{-1}\log(Z(x;\tilde{x}=0))$, where $l^2/a^2 = 0.04$ and $Z(x;\tilde{x}=0)$ was obtained by Eq. (**??**) with $I = 30$. Horizontal lines represent the first few energy levels. Note that the three lowest levels are all nearly twofold degenerate. (b) Comparison between $F(x,\tilde{x}=0)$ and the results of metadynamics. (c) Comparison between $P(X;\tilde{X}=0)$ (Eq. (**??**)), $I = 30$, and the ground state probability density $|\Psi_0(x;\tilde{x}=0)|^2$. Panel (d): Comparison between $P(X;\tilde{X}=0)$ and the constrained partition function resulting from metadynamics (normalized). Parameters for the metadynamics simulation are the following: $P = 10$, total number of Gaussians $N_{\mathrm{tot}} = 300000$, $w = 0.01\hbar\omega$, $\tau_G = 20000$, $\Delta T = 8\hbar\omega/k_{\mathrm{B}}$, $\sigma_x = 0.05$, $\sigma_{E_K} = 0.02$

where

$$\gamma_{\mathrm{wtm}} = \frac{T+\Delta T}{T}$$

is the so-called *bias factor*. Furthermore, it is possible to obtain an asymptotically time-independent estimator of the free-energy [**?**] that can be used both to compare metadynamics simulations with different parameters and estimate the degree of convergence of any given free-energy basin:

$$F(\mathbf{S},t_{\mathrm{MC}}) = -\frac{\gamma_{\mathrm{wtm}}}{k_{\mathrm{B}}\Delta T}V_{\mathrm{wtm}}(\mathbf{S},t_{\mathrm{MC}}) + \frac{1}{\beta}\log\int \mathrm{d}\mathbf{S}'\exp\left(\frac{T+\Delta T}{\Delta T}\beta V_{\mathrm{wtm}}(\mathbf{S}',t_{\mathrm{MC}})\right). \tag{3.66}$$

The idea behind metadynamics is that of "filling free-energy basins with gaussians", this intuitive mechanism can be given a rigorous definition if we

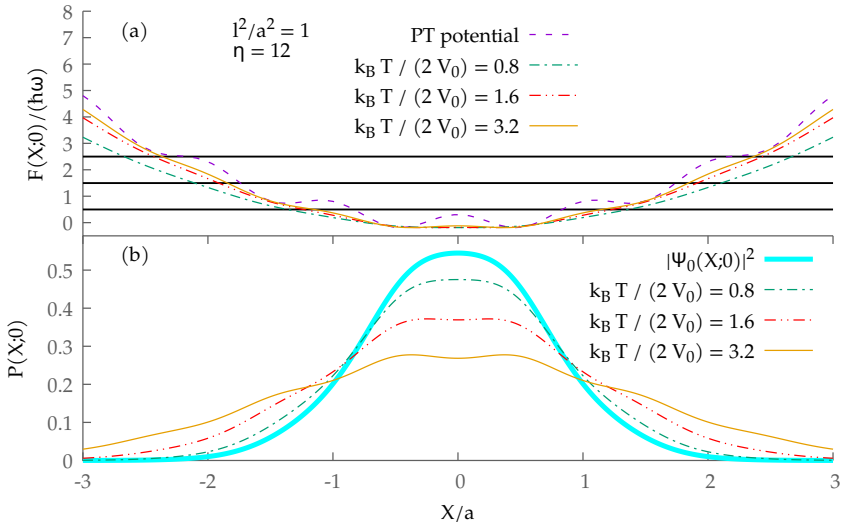

Figure 3.13: Panel (a): Comparison between the classical PT potential $V_{\mathrm{PT}}(x;\tilde{x})$ and the constrained free energy $F_P(x;\tilde{x}) = -1/\beta \log(Z_P(x;\tilde{x}))$, where $l^2/a^2 = 1$ and $Z_P(x;\tilde{x})$ was obtained by Eq. (**??**) with $I = 30$. Horizontal lines represent the first few energy levels. Panel (b): Comparison between $P(X;\tilde{X})$ (Eq. (**??**)), $I = 30$, and the ground state probability density $|\Psi_0(x;\tilde{x})|^2$.

think of it as a procedure to transition between two probability distributions:

$$P_0(\mathbf{S}) = \frac{\exp\left(-\beta F(\mathbf{S})\right)}{Z} \rightarrow P_{\mathrm{meta}}(\mathbf{S}); \tag{3.67}$$

in other words "filling the free-energy basins" implies that when the metadynamics procedure is completed we expect the FES to be flat, and therefore the probability distribution $P_{\mathrm{meta}}(\mathbf{S})$ to be uniform [**?**]. The well-tempered variant of metadynamics can be given a similar interpretation as a procedure to transition from the Boltzmann distribution to a smoother one, call it $P_{\mathrm{wtm}}(\mathbf{S})$, such that free-energy barriers are lowered by a factor of $\gamma = (T + \Delta T)/T$. For concreteness, from now on let us focus on the well-tempered scheme. During the simulation the probability distribution will not be exactly $P_{\mathrm{wtm}}(\mathbf{S})$, but we know that:

$$\lim_{t_{\mathrm{MC}} \rightarrow \infty} P_{\mathrm{wtm}}(\mathbf{S}, t_{\mathrm{MC}}) = P_{\mathrm{wtm}}(\mathbf{S}), \tag{3.68}$$

If we can estimate $P_{\mathrm{wtm}}(\mathbf{S}, t_{\mathrm{MC}})$, given an operator $\hat{O}$ we can also calculate its average value by collecting statistics of the trajectory explored during the well-tempered metadynamics simulation [**?**]. Indeed:

$$\begin{aligned} \left\langle \hat{O} \right\rangle &= \int \mathrm{d}\mathbf{x} O(\mathbf{x}) P_0(\mathbf{x}) = \int \mathrm{d}\mathbf{x} O(\mathbf{x}) P_{\mathrm{wtm}}(\mathbf{S}(\mathbf{x}), t_{\mathrm{MC}}) \frac{P_0(\mathbf{x})}{P_{\mathrm{wtm}}(\mathbf{S}(\mathbf{x}), t_{\mathrm{MC}})} \\ &= \int \mathrm{d}X O(\mathbf{x}) w(\mathbf{x}, t_{\mathrm{MC}}) P_{\mathrm{wtm}}(\mathbf{S}(\mathbf{x}), t_{\mathrm{MC}}) = \left\langle \hat{O} w(\mathbf{x}, t_{\mathrm{MC}}) \right\rangle_{\mathrm{wtm}}, \end{aligned} \tag{3.69}$$

where

$$w(\mathbf{x}, t_{\mathrm{MC}}) = \frac{P_0(\mathbf{S}(\mathbf{x}))}{P_{\mathrm{wtm}}(\mathbf{S}(\mathbf{x}), t_{\mathrm{MC}})}. \tag{3.70}$$

Given a way to compute these weights we can compute average values of any observable as weighted averages over the biased MC trajectory $\{\mathbf{x}_j\}_{j=1}^{J} =$

$\{(x_{1j}, \dots, x_{Pj})\}_{j=1}^{J}$, with the same notation as Eq. (**??**):

$$\left\langle \hat{O} \right\rangle \approx \frac{\sum_{j=1}^{J} O(X'_{1j}) w(X'_{1j}, j)}{\sum_{j=1}^{J} w(X'_{1j}, j))}. \tag{3.71}$$

This procedure is called "reweighting". Many ways to estimate $w(\mathbf{x}, t_{\mathrm{MC}})$ have been proposed over the years [**?**, **?**, **?**, **?**], we implement[**?**] the one proposed by Tiwary and Parrinello [**?**]:

$$w(\mathbf{x}, t_{\mathrm{MC}}) = \frac{\exp\left(\beta V_{\mathrm{wtm}}(\mathbf{S}(\mathbf{x}), t_{\mathrm{MC}})\right)}{\left\langle \exp\left(\beta V_{\mathrm{wtm}}(\mathbf{S}(\mathbf{x}), t_{\mathrm{MC}})\right)\right\rangle_{\mathrm{wtm}}}, \tag{3.72}$$

so that average values of observables are reweighted according to the following scheme:

$$\left\langle \hat{O} \right\rangle = \left\langle \hat{O} \exp\left(\beta V_{\mathrm{wtm}}(\mathbf{S}(\mathbf{x}), t_{\mathrm{MC}}) - c(t_{\mathrm{MC}})\right)\right\rangle_{\mathrm{wtm}}, \tag{3.73}$$

where

$$c(t_{\mathrm{MC}}) = \frac{1}{\beta} \log \frac{\int \mathrm{d}\mathbf{S}' \exp\left(-\beta F(\mathbf{S}')\right)}{\int \mathrm{d}\mathbf{S}' \exp\left(-\beta (F(\mathbf{S}') + V_{\mathrm{wtm}}(\mathbf{S}', t_{\mathrm{MC}}))\right)}. \tag{3.74}$$

and we substitute $F(\mathbf{S})$ with its well-tempered estimate Eq. (**??**):

$$c(t_{\mathrm{MC}}) = \frac{1}{\beta} \log \frac{\int \mathrm{d}\mathbf{S}' \exp\left(\frac{\gamma_{\mathrm{wtm}}}{k_{\mathrm{B}}\Delta T} V_{\mathrm{wtm}}(\mathbf{S}', t_{\mathrm{MC}})\right)}{\int \mathrm{d}\mathbf{S}' \exp\left(\frac{V_{\mathrm{wtm}}(\mathbf{S}', t_{\mathrm{MC}})}{k_{\mathrm{B}}\Delta T}\right)}. \tag{3.75}$$

Having computed $F_P(x, E_K; \tilde{x})$ one can compare the result to the classical FES by logarithmically integrating out K:

$$F_P(x; \tilde{x}) = -\frac{1}{\beta} \log \left\{ \int \mathrm{d}E_K \exp\left(-\beta F_P(x, E_K; \tilde{x})\right) \right\} \xrightarrow{P\to\infty} F(x; \tilde{x}) \tag{3.76}$$

In the high-temperature limit the Trotter splitting is exact and therefore the quantum FES should approximate the classical PT potential (Eq. (**??**)):

$$F(X; \tilde{X}) = F(lx; l\tilde{x}) \xrightarrow{T\to\infty} V_{\mathrm{PT}}(X; \tilde{X}). \tag{3.77}$$

On the other hand, in the low-temperature limit the probability density should converge to the ground state probability density $|\Psi_0(X; \tilde{X})|^2$:

$$P(X; \tilde{X}) = \frac{Z(X; \tilde{X})}{\int_{\mathbb{R}} \mathrm{d}x Z(x; \tilde{x})} = \frac{Z(lx; l\tilde{x})}{\int_{\mathbb{R}} \mathrm{d}x Z(x; l\tilde{x})} \xrightarrow{T\to 0} |\Psi_0(X; \tilde{X})|^2. \tag{3.78}$$

In general one can compare the probability density associated to the calculated FES to the probability density given by the thermal mixing of the first I eigenstates:

$$P(x; \tilde{x}) = \frac{Z(x; \tilde{x})}{\int_{\mathbb{R}} \mathrm{d}x Z(x; \tilde{x})} \approx \frac{\sum_{i=0}^{I} \mathrm{e}^{-\beta E_i(\tilde{x})} |\Psi_i(x; \tilde{x})|^2}{\sum_{i=0}^{I} \exp\left(-\beta E_i(\tilde{x})\right)}, \tag{3.79}$$

where $\Psi_i(x;\tilde{x})$ is the i-th eigenstate of the Hamiltonian at fixed $\tilde{x}$, see Fig. **??**. Provided that I is chosen so that $E_I(\tilde{x}) - E_0(\tilde{x}) \gg k_B T$. We can then compare the results of metadynamics with the probability density obtained by explicit diagonalization, see Fig. **??**(b)-(d). In accordance with the previous section, quantum-mechanical effects reduce the effective barriers and, in the strongly quantum mechanical regime, even remove them completely.

Having introduced PIMC and metadynamics, we will now show how they can be used to compute the quantity of interest:

$$-\chi = \left.\frac{\partial^2 F(\tilde{X})}{\partial \tilde{X}^2}\right|_{\tilde{X}=0}. \tag{3.80}$$

By definition $Z(\tilde{x}) = -1/\beta \log F(\tilde{x})$, which implies:

$$\frac{\partial F(\tilde{x})}{\partial \tilde{x}} = -\frac{1}{\beta}\frac{1}{Z(\tilde{x})}\frac{\partial Z(\tilde{x})}{\partial \tilde{x}}. \tag{3.81}$$

Substituting the definition of $Z(\tilde{x})$, Eq. (**??**), we obtain:

$$\frac{\partial \log Z(\tilde{x})}{\partial \tilde{x}} = \lim_{P\to\infty} \int \mathrm{d}\mathbf{x}\, P_P(\mathbf{x};\tilde{x}) \frac{\beta\hbar\omega}{P} \sum_{p=1}^{P} (x_p - \tilde{x}). \tag{3.82}$$

This quantity is sufficient to compute the second derivative:

$$\begin{aligned}\frac{\partial^2 F(\tilde{x})}{\partial \tilde{x}^2} = \lim_{P\to\infty} \frac{1}{\beta} \Bigg\{ \Bigg[\int \mathrm{d}\mathbf{x}\, P_P(\mathbf{x};\tilde{x}) \frac{\beta\hbar\omega}{P} \sum_{p=1}^{P} (\tilde{x} - x_p) \Bigg]^2 - \\ \int \mathrm{d}\mathbf{x}\, P_P(\mathbf{x};\tilde{x}) \left[\frac{(\beta\hbar\omega)^2}{P^2} \sum_{p,p'=1}^{P} (x_p - \tilde{x})(\tilde{x} - x_{p'}) - \beta\hbar\omega \right] \Bigg\}\end{aligned} \tag{3.83}$$

Unfortunately, due to time constraints, we were not able to test the Path Integral Monte Carlo method to compute this quantity.

Chapter 4

Conclusions and outlook

In this thesis we propose a novel semi-quantitative method to infer kinetic frictional properties for the classical and quantum Prandtl-Tomlinson model based on equilibrium averages. We focus on the free energy F for both the classical and the quantum PT model, and observe that the stick-slip regime requires a sharp cusp-like shape of this thermodynamical quantity as the PT slider traverses a maximum point of the periodic potential, see Fig. **??**. This sharp cusp signals a rapid sign switch of the force acting on the PT slider, when crossing to the next attraction basin. Accordingly, we evaluate the second derivative

$$-\chi = \left.\frac{\partial^2 F(\tilde{X})}{\partial \tilde{X}^2}\right|_{\tilde{X}=0}, \tag{4.1}$$

which has to be negative and large for stick-slip dynamics to be expected at least in a suitable driving velocity range. We use classical dynamical simulations to estimate the value χ_c where a crossover from stick-slip to smooth/thermolubric dynamics occurs, see Figs. **??**, **??**. In other terms, for $\chi = |\partial^2 F(\tilde{X}=0)/\partial \tilde{X}^2| < \chi_c$, smooth/thermolubric sliding is expected to occur at any speed.

While thermal effects are quantified by the ratio between the temperature and the barrier height $k_B T/(2V_0)$, we gauge quantum effects by the squared ratio between the oscillator length and the periodicity of the substrate potential $(l/a)^2 = \hbar\omega/(Ka^2)$. The effects of quantum mechanics and temperature are both to decrease χ, but in quite different ways: The approach to the classical deterministic $T = 0$ limit is $\chi \propto \beta \propto T^{-1}$ in the classical model, see Eq. (**??**) and Fig. **??**, while it is exponential in $(a/l)^2$ for the quantum ground state as "quantumness" decreases, see Fig. (**??**). We predict that thermal/quantum effects will decrease χ below χ_c, thus getting rid of the stick-slip dynamics for sufficiently high temperature and/or sufficiently strong "quantumness".

Future research directions include:

- Perfecting the classical analysis described in Sec. **??**, investigating the precise quantitative link between χ_c and the corresponding temperature;
- Correcting the estimates of the derivative of the ground-state energy

$$\left.\frac{\partial^2 E_0(\tilde{X})}{\partial \tilde{X}^2}\right|_{\tilde{X}=0}, \tag{4.2}$$

by employing, e.g., the WKB approximation;

- Estimating friction [**?**] taking not just thermal but also quantum effects into consideration, e.g. by evaluating tunneling rates through the WKB method [**?**];
- Thoroughly testing the PIMC approach described in Sec. **??** and applying it to an extended PT model that accounts explicitly for the phononic excitations, both in the classical and quantum regimes. Appendix **??** reports preliminary calculations for the PT model coupled to an harmonic chain.

Appendix A

Partition function for the classical PT model

In this appendix we calculate a useful approximation for the partition function of the classical PT model, introduced in **??**:

$$\begin{aligned} Z(\tilde{X}) &= \int_{\mathbb{R}^2} \frac{\mathrm{d}X\mathrm{d}P}{2\pi\hbar} \mathrm{e}^{-\beta\left(\frac{P^2}{2M}+V_{\mathrm{PT}}(X,\tilde{X})\right)} = \int_{\mathbb{R}} \frac{\mathrm{d}X}{\Lambda} \mathrm{e}^{-\beta V_{\mathrm{PT}}(X,\tilde{X})} = \\ &= \frac{a}{\Lambda} \int_{\mathbb{R}} \mathrm{d}x \exp\left[-\beta K a^2 \frac{x^2}{2} - \beta V_0 \cos(2\pi(x+\tilde{x}))\right], \end{aligned} \tag{A.1}$$

in the last step we carried out the substitution $x = (X - \tilde{X})/a$ and introduced the thermal length Λ defined in Eq. (**??**) and the dimensionless slider position $\tilde{x} = \tilde{X}/a$. Calculating the partition function Eq. **??** reduces to the following integral:

$$Z(\tilde{x}) = \frac{a}{\Lambda} \int_{\mathbb{R}} \mathrm{d}x \exp\left(-\frac{x^2}{2\sigma^2}\right) \mathrm{e}^{-b\cos(2\pi(x+\tilde{x}))}, \tag{A.2}$$

with

$$\sigma^2 = 1/(\beta K a^2), \quad b = \beta V_0 \ .$$

We can simplify the problem by restricting our attention to the low temperature regime $T \to 0$, $\beta V_0 = b \to \infty$, where we expect the second derivative of the free energy to diverge, see **??**. In order to extract the asymptotic behavior of Eq. (**??**) we can expand the second exponential in Fourier series:

$$\mathrm{e}^{-b\cos(2\pi(x+\tilde{x}))} = \mathrm{e}^{b\cos(2\pi(x+\tilde{x})+\pi)} = \sum_{n=-\infty}^{+\infty} I_n(b) \mathrm{e}^{in2\pi(x+\tilde{x})} \mathrm{e}^{in\pi}, \tag{A.3}$$

where the Fourier components $I_n(b)$ are the modified Bessel functions of the first kind:

$$I_n(b) = \int_{-\pi}^{\pi} \frac{\mathrm{d}\theta}{2\pi} \mathrm{e}^{-in\theta} \exp(b\cos\theta). \tag{A.4}$$

Substituting the series expansion and exchanging the series and the integral we obtain:

$$\begin{aligned} Z(\tilde{x}) &= \frac{a}{\Lambda}\sum_{n\in\mathbb{Z}} I_n(b)\int_{\mathbb{R}} \mathrm{d}x \exp\left(-\frac{x^2}{2\sigma^2}\right)\mathrm{e}^{in\pi}\mathrm{e}^{i2\pi n(x+\tilde{x})} = \\ &= \frac{a}{\Lambda}\sum_{n\in\mathbb{Z}} (-1)^n I_n(b)\mathrm{e}^{i2\pi n\tilde{x}}\int_{\mathbb{R}} \mathrm{d}x \exp\left(-\frac{x^2}{2\sigma^2}+i2\pi n x\right) = \\ &= \frac{a}{\Lambda}\sum_{n\in\mathbb{Z}} \sqrt{2\pi\sigma^2}(-1)^n I_n(b)\mathrm{e}^{-2\pi^2n^2\sigma^2}\mathrm{e}^{i2\pi n\tilde{x}} = \\ &= \frac{a}{\Lambda}\sqrt{2\pi\sigma^2}\left(I_0(b)+2\sum_{n=1}^{+\infty}(-1)^n I_n(b)\cos(2\pi n\tilde{x})\mathrm{e}^{-2\pi^2n^2\sigma^2}\right). \end{aligned} \tag{A.5}$$

Going back to the definition of the modified Bessel functions $I_n(b)$, Eq. (**??**), we notice that for $b\to\infty$ the integral is dominated by the regions close to the maxima of $\cos\theta$. We now (i) expand $\cos\theta \approx 1-\theta^2/2$ in the small-$|\theta|$ region (thereby renouncing the periodicity in θ, and therefore in $\tilde{x}$), and (ii) extend the integration to the entire real line, as appropriate for large b (i.e. large βV_0):

$$\begin{aligned} I_n(b) &\overset{\text{(i)}}{\simeq} \int_{-\pi}^{+\pi}\frac{\mathrm{d}\theta}{2\pi}\mathrm{e}^{-in\theta}\mathrm{e}^{b(1-\theta^2/2)} \\ &\overset{\text{(ii)}}{\simeq} \mathrm{e}^b\int_{-\infty}^{+\infty}\frac{\mathrm{d}\theta}{2\pi}\exp\left(-b\frac{\theta^2}{2}-in\theta\right) = \\ &= \frac{\mathrm{e}^b}{\sqrt{2\pi b}}\exp\left(-\frac{n^2}{2b}\right). \end{aligned} \tag{A.6}$$

Substituting back

$$\sigma^2 = \frac{1}{\beta K a^2} = \frac{1}{b}\frac{\eta}{4\pi^2}, \quad b = \beta V_0,$$

and the asymptotic expression for $I_n(b)$ for $b\to\infty$, Eq. (**??**) reads:

$$\begin{aligned} Z(\tilde{x}) &= \frac{a}{\Lambda}\int_{\mathbb{R}}\mathrm{d}x\exp\left(-\beta K a^2\frac{x^2}{2}-\beta V_0\cos(2\pi(x+\tilde{x}))\right) = \\ &\overset{\beta V_0\to\infty}{\simeq} \sqrt{\eta}\frac{\mathrm{e}^{\beta V_0}}{2\pi\beta V_0}\left[1+2\sum_{n=1}^{+\infty}(-1)^n\exp\left(-\frac{n^2}{2\beta V_0}(\eta+1)\right)\cos(2\pi n\tilde{x})\right] = \\ &= \sqrt{\eta}\frac{\mathrm{e}^{\beta V_0}}{2\pi\beta V_0}\theta_4\left(\tilde{x};\exp\left(-\frac{\eta+1}{2\beta V_0}\right)\right), \end{aligned} \tag{A.7}$$

where we recognized the term in square brackets as the Jacobi theta function of the fourth kind [**?**]:[1]

$$\theta_4(z;q) = 1+2\sum_{n=1}^{\infty}(-1)^n q^{n^2}\cos(2\pi n z). \tag{A.8}$$

In the literature q is called the *nome* and often expressed as:

$$q = \mathrm{e}^{i\pi\tau}. \tag{A.9}$$

[1] The notation one finds in the literature for θ_4 is fairly standardized, although disputable. Other than the definition in Eq. (**??**), one also finds the following definition of θ_4:

$$\theta_4(z,q) = \theta_4\left(\frac{z}{\pi};q\right),$$

which differs by a factor of π and the use of a comma (',') rather than a semicolon (';'). In order to avoid confusion, we chose to adopt the definition that mostly resembles the series we obtain for $Z(\tilde{x})$, nevertheless care must be taken in order to keep track of the correct factors of π when comparing with the literature. To further reduce the possibility of confusion, we adopt the customary names for the variables z, q and τ.

In order to obtain an asymptotic expansion for $\theta_4(z;q)$ as $q \to 1^-$, or alternatively $\theta_4^\tau(z;\tau) := \theta_4(z;e^{i\pi\tau})$ for $\tau \to i0^+$, we can exploit the symmetries of the Jacobi theta function under the *modular transformation* $\tau \to -1/\tau$:

$$\theta_4^\tau(z;\tau) = \frac{\exp\left(-\frac{i\pi z^2}{\tau}\right)}{\sqrt{-i\tau}}\theta_2^\tau\left(\frac{z}{\tau};-\frac{1}{\tau}\right), \tag{A.10}$$

where

$$\theta_2^\tau(z;\tau) = \sum_{n=-\infty}^{+\infty} e^{i\pi\tau(n+1/2)^2}e^{i(2n+1)\pi z}. \tag{A.11}$$

The modular transformation $\tau \to -1/\tau$ maps the behaviour of θ_4 for $q \to 1^-$ to the behaviour of θ_2 for $q \to 0$ where the series converges quickly and can be accurately approximated by the leading terms. Indeed, by using Eq. (**??**) and Eq. (**??**) we can write:

$$\begin{aligned}\theta_4^\tau(z;\tau) &= \frac{\exp\left(-\frac{i\pi z^2}{\tau}\right)}{\sqrt{-i\tau}}\theta_2^\tau\left(\frac{z}{\tau};-\frac{1}{\tau}\right) = \\ &= \frac{\exp\left(-\frac{i\pi z^2}{\tau}\right)}{\sqrt{-i\tau}}\sum_{n=-\infty}^{+\infty}\exp\left(-\frac{i\pi}{\tau}(n+1/2)^2\right)\exp\left(i(2n+1)\frac{\pi z}{\tau}\right) = \\ &\overset{\tau\to i0^+}{\simeq} \frac{\exp\left(-\frac{i\pi z^2}{\tau}\right)}{\sqrt{-i\tau}}\exp\left(\frac{\pi}{4i\tau}\right)\left[e^{\frac{i\pi z}{\tau}} + e^{-\frac{i\pi z}{\tau}}\right].\end{aligned} \tag{A.12}$$

We can then rewrite this in terms of q via Eq. (**??**):

$$\theta_4(z;q) = 2\sqrt{\frac{\pi}{\log(1/q)}}\exp\left(\frac{\pi^2 z^2}{\log q}\right)\exp\left(\frac{\pi^2}{4\log q}\right)\cosh\left(\frac{\pi^2 z}{\log q}\right), \tag{A.13}$$

With this asymptotic expansion and the identification

$$z = \tilde{x}, \quad q = \exp\left(-\frac{\eta+1}{2\beta V_0}\right), \tag{A.14}$$

the partition function reads:

$$Z(\tilde{x}) \overset{\beta V_0\to\infty}{\simeq} 2\frac{a}{\Lambda}\sqrt{\frac{\eta}{\eta+1}}\frac{e^{\beta V_0}}{\sqrt{2\pi\beta V_0}}\exp\left(-\frac{2\pi^2\beta V_0}{\eta+1}(\tilde{x}^2+1/4)\right)\cosh\left(\frac{2\pi^2\beta V_0\tilde{x}}{\eta+1}\right). \tag{A.15}$$

As show in Fig. **??** the asymptotic result of Eq. (**??**) agrees fairly well with the free energy surface obtained by numerical integration[**?**] of Eq. (**??**) for temperatures as high as $10^{-1}V_0/k_B$.

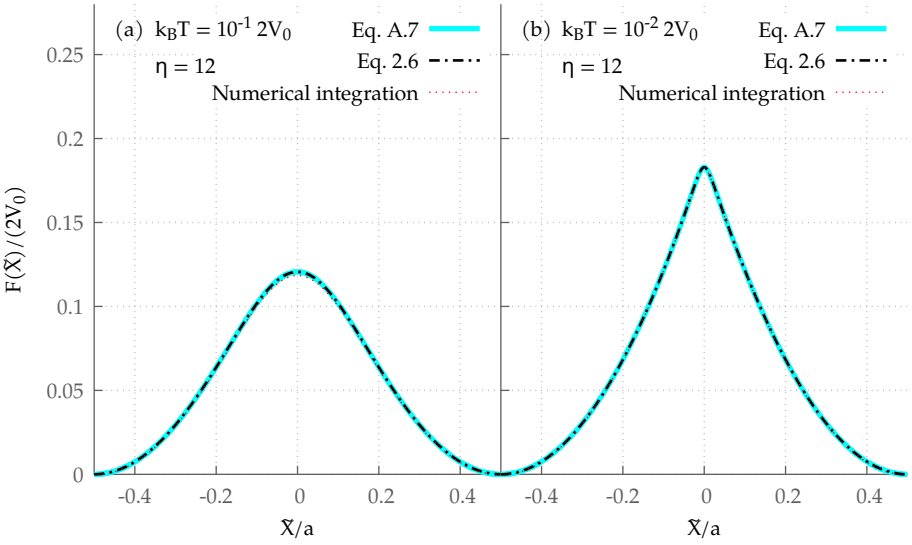

Figure A.1: Comparison between the free energy surface obtained by numerical integration of Eq. (**??**) (dashed lines), by the asymptotic expansion Eq. (**??**) (dot-dashed line) and by summing the series in Eq. (**??**) (solid lines), for $\eta = 12$ and (a) $k_BT/(2V_0) = 0.1$, (b) $k_BT/(2V_0) = 0.01$. As expected, the agreement improves in the $T \to 0$ limit.

Appendix B

Validating the metadynamics procedure

Before applying the procedure described in Section **??**, we validate it by testing it on simple or analytically solvable quantum systems. The focus of this section is calculating free energy surfaces, i.e. equilibrium distributions for quantum observables of interest. Given a 1D system with Hamiltonian $\hat{H}$, its equilibrium state is:

$$\rho = \frac{\mathrm{e}^{-\beta\hat{H}}}{Z}. \tag{B.1}$$

Given an observable $A(\hat{x})$, we can calculate its average value:

$$\langle A \rangle = \mathrm{Tr}\left\{\rho\hat{A}\right\} = \int_{\mathbb{R}} \mathrm{d}x \rho(x,x) A(x), \tag{B.2}$$

furthermore by inserting an identity $\int \mathrm{d}A\delta(A - A(x))$ and exchanging the order of integration we obtain:

$$\langle A(\hat{x}) \rangle = \int_{\mathbb{R}} \mathrm{d}A \mathrm{e}^{-\beta F(A)} A, \quad F(A) := -\frac{1}{\beta} \log\left(\int_{\mathbb{R}} \mathrm{d}x \delta(A - A(x)) \rho(x,x)\right). \tag{B.3}$$

Metadynamics and Path-Integral Monte Carlo can be used to calculate both the average value $\langle A(\hat{x}) \rangle$ and the equilibrium distribution $F(A)$.

B.1 The quantum harmonic oscillator

By far the most studied quantum system is the 1 dimensional quantum harmonic oscillator (QHO), governed by the Hamiltonian:

$$\hat{H}_{\mathrm{QHO}} = \hbar\omega\left(\frac{1}{2}\hat{p}^2 + \frac{1}{2}\hat{x}^2\right). \tag{B.4}$$

The density matrix of the quantum harmonic oscillator can be calculated analytically:

$$\rho_{\mathrm{QHO}}(x,x) = \mathrm{e}^{-\beta F(x)}, \quad \frac{F(x)}{\hbar\omega} = \frac{T}{T_{\mathrm{vib}}} \tanh\left(\frac{T_{\mathrm{vib}}}{2T}\right) x^2, \tag{B.5}$$

where $T_{\mathrm{vib}} = \hbar\omega/k_{\mathrm{B}}$. This analytic result is compared to the harmonic potential

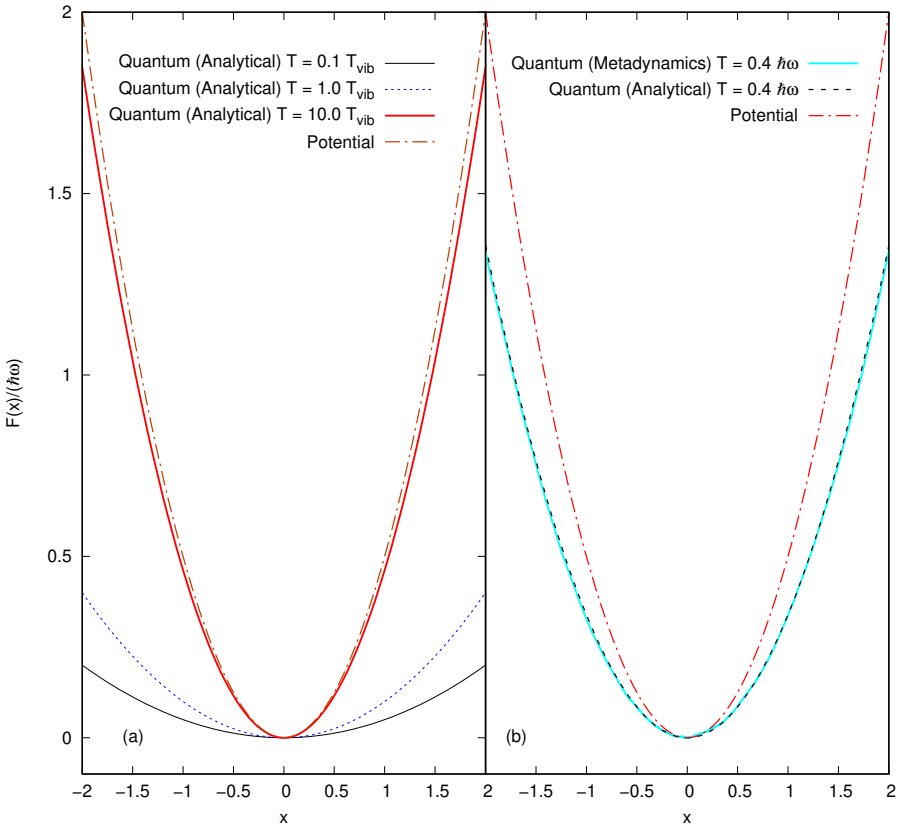

Figure B.1: Panel (a): Free energy for the QHO, Eq. (**??**), compared to the potential $\hbar\omega/2\,x^2$. Panel (b): Comparison between the free energy calculated as in Section **??** (cyan, solid), the quantum free energy Eq. (**??**) (black, dashes) and the potential (red, dashes and dots). Parameters for the metadynamics simulation: $N_{\text{gaus}} = 100000$, $h = 0.01\hbar\omega$, $\sigma_X = 0.3$, $\sigma_K = 0.05$, simulation box $[-5, 5]$, $N_{\text{delay}} = 10000$, $P = 10$ ($P_{\text{min}} = 1$), $T = 0.4T_{\text{vib}}$, $\Delta T = 3$.

in Fig. **??**a. The QHO does not present any of the features that make metadynamics useful: there are no energy barriers to overcome, nor competing local minima to explore, but its simplicity and the availability of an analytic solution for F make it a sensible test system. As shown in Fig. **??**b, the metadynamics calculation reliably reproduces the expected FES.

B.2 The double well

A more interesting quantum system that exhibits the features we would like to benchmark in metadynamics calculations is the double well (DW), a system governed by Hamiltonian:

$$\hat{H}_{\text{DW}} = \frac{\hbar}{2M}\hat{p}^2 + B\left(\hat{x}^4 - 2\hat{x}^2 + 1\right). \tag{B.6}$$

The potential, depicted in Fig. **??**, is characterized by two minima at $x = -1$ and $x = 1$ separated by a barrier of height B. When the barrier is of the order of unity we expect tunneling between the two minima and therefore slight decrease in the effective barrier height, this is indeed the case for $T = 0.4$ (in natural units) as the metadynamics calculations show in Fig. **??**. The thermal

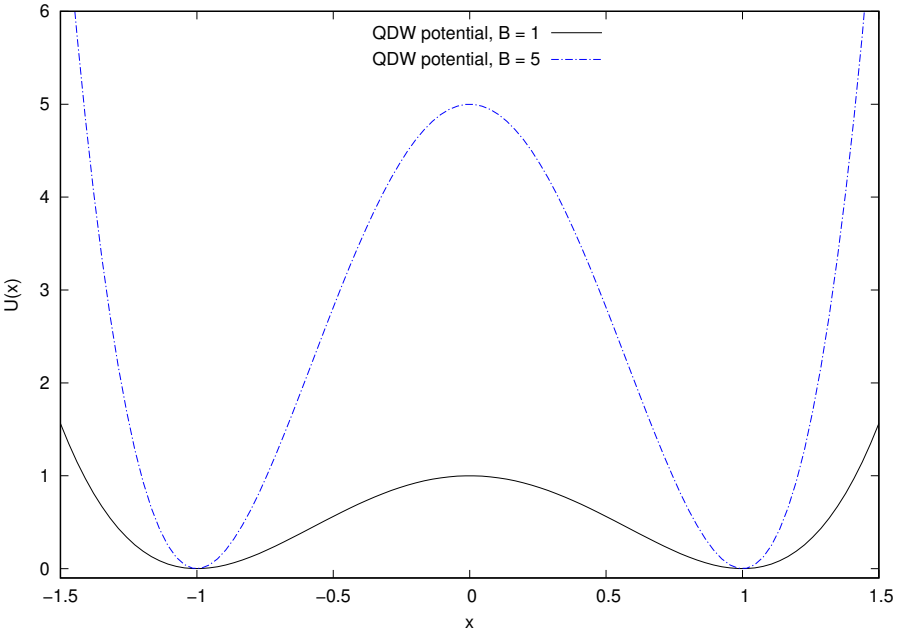

e potential energy for
$B(x^4 - 2x^2 + 1)$.

In the following we rescale our units so that $\hbar = M = 1$:

$$\hat{H}_{\mathrm{DW}} = \frac{1}{2}\hat{p}^2 + B\left(\hat{x}^4 - 2\hat{x}^2 + 1\right). \tag{B.7}$$

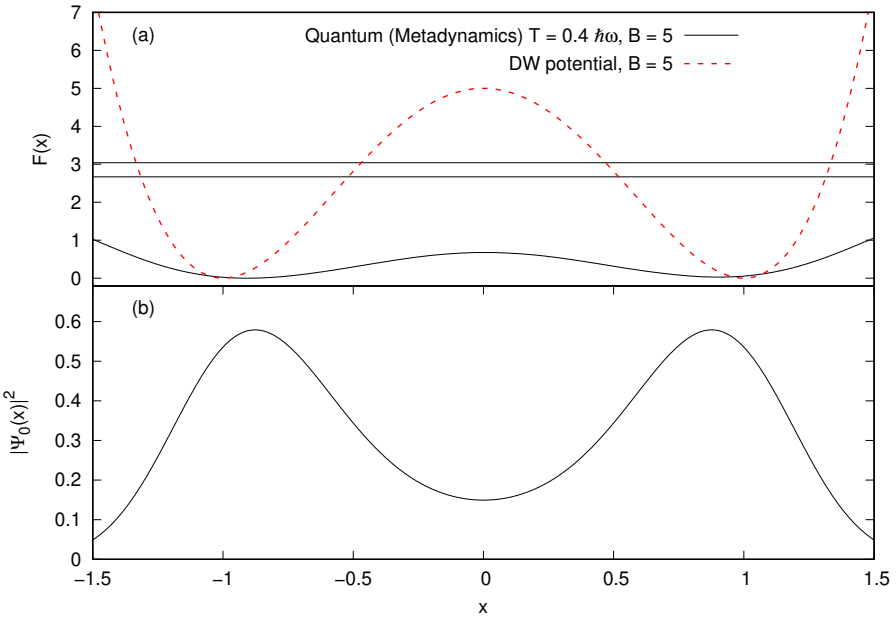

Panel (a): Compari-
quantum FES (black,
he DW potential (red,
ontal lines mark the
els of the system, both
nd their position be-
mark the presence of
neters for the metady-
on: $N_{\mathrm{gaus}} = 150000$,
$= 0.3$, $\sigma_K = 0.05$,
$T = 0.4$, $P = 100$,
el (b): Ground state
ity $|\Psi_0(x)|^2$ for $B = 5$,
corresponding to the
$\Psi_0(x)|^2 \neq 0$ is a stark
esence of tunneling.

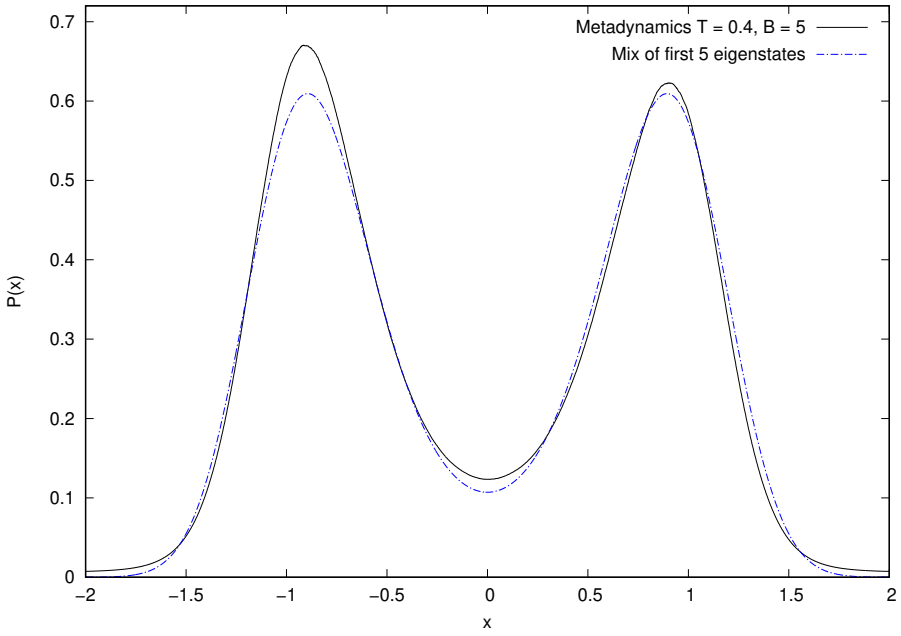

Figure B.4: Comparison of the probability density obtained by metadynamics Eq. (**??**) (black, solid line) with the approximate probability density $\rho^M_{\mathrm{DW}}(x)$ for $I = 5$ (blue, dots and dashes). Parameters for metadynamics are as in Fig. **??**. As shown in Fig. **??**, metadynamics is very sensitive to the addition of Gaussians near the free energy minima, so that the maximum error will coincide with the peaks in the probability distribution.

Gibbs state for this quantum system is:

$$\hat{\rho_{\mathrm{DW}}} = \frac{1}{Z}\exp\left(-\frac{\hat{H}_{\mathrm{DW}}}{T}\right) = \frac{\sum_n \mathrm{e}^{-E_n/T}\,|\Psi_n\rangle\langle\Psi_n|}{\sum_n \mathrm{e}^{-E_n/T}}, \tag{B.8}$$

where Ψ_n and E_n are eigenvectors and eigenvalues of $\hat{H}_{\mathrm{DW}}$, solutions to the stationary Schödinger equation:

$$\hat{H}_{\mathrm{DW}}\Psi_n = E_n\Psi_n. \tag{B.9}$$

We can compare the probability density associated to the FES, i.e.

$$P(x) = \frac{\exp\left(-\frac{F(x)}{T}\right)}{\int \mathrm{d}x \exp\left(-\frac{F(x)}{T}\right)}, \tag{B.10}$$

to the diagonal part of the integral kernel $\rho_{\mathrm{DW}}(x, y)$:

$$\rho_{\mathrm{DW}}(x) = \frac{1}{Z}\langle x|\rho_{\mathrm{DW}}|x\rangle = \frac{1}{Z}\sum_n \mathrm{e}^{-E_n/T}|\Psi_n(x)|^2. \tag{B.11}$$

In practice we can solve the 1-dimensional Schrödinger equation numerically for the first N eigenvalues and eigenvectors and then approximate Eq. (**??**) by:

$$\rho^N_{\mathrm{DW}}(x) = \frac{\sum_n^N \mathrm{e}^{-E_n/T}|\Psi_n(x)|^2}{\sum_n^N \mathrm{e}^{-E_n/T}}, \tag{B.12}$$

the result of this comparison is shown in Fig. **??**.

Appendix C

The shooting method

Consider a 1D Schrödinger differential operator:

$$\hat{H} = -\frac{1}{2}\frac{\mathrm{d}^2}{\mathrm{d}x^2} + V(x) \tag{C.1}$$

and its associated eigenvalue problem:

$$\left[-\frac{1}{2}\frac{\mathrm{d}^2}{\mathrm{d}x^2} + V(x)\right]\psi_i(x) = E_i\psi_i(x). \tag{C.2}$$

Implicit in the statement of the eigenvalue equation is that $\psi_i(x) \in L^2(\mathbb{R})$ which implies:

$$\psi_i(x) \xrightarrow{|x|\to\infty} 0. \tag{C.3}$$

The shooting method [**?**, **?**] is an iterative algorithm to compute both E_i and $\psi_i(x)$ by solving an initial value problem associated to the eigenvalue equation. The algorithm is based on the following well-known properties of the eigenvalues E_i and eigenstates $\psi_i(x)$:

- Eigenvalues are ordered: $\forall j, i \in \mathbb{N} : i < j \implies E_i \leq E_j$, this is not really a property, but rather a useful naming convention,
- Eigenstates are exponentially localized, i.e. $\psi_i(x) \overset{x\to\pm\infty}{\sim} \exp\left(\mp\beta_\pm x\right)$ for $\beta_\pm > 0$,
- The index $i \in \mathbb{N}$ of the eigenstate $\psi_i(x)$ corresponds to the number of nodes of $\psi_i(x)$.

These three facts are sufficient to state the core of the shooting method to solve Eq. **??** for a given eigenvalue and eigenstate pair $(E_i, \psi_i(x))$:

1. Select an interval $I = [a, b] \subset \mathbb{R}$ sufficiently large so that $\psi_i(a) \approx 0$ and $\psi_i(b) \approx 0$ (this is guaranteed to exist by virtue of the exponential localization of the eigenstates) and define:

$$E_m = \min_{x\in I} V(x), \quad E_M = \max_{x\in I} V(x), \quad E = \frac{E_m + E_M}{2}, \tag{C.4}$$

   It is important to note that the interval $[E_m, E_M]$ must contain E_i for the algorithm to work,

2. Solve the initial value problem:

$$\begin{cases} \psi(a) = 0 \\ \left[-\frac{1}{2}\frac{\mathrm{d}^2}{\mathrm{d}x^2} + V(x)\right]\psi(x) = E\psi(x), \end{cases} \tag{C.5}$$

   by discretizing the interval I and integrating the differential equation with e.g. the Numerov algorithm.

3. Count the number of nodes N of f, if $N > i$ than the trial eigenvalue E is too high, otherwise it is too low. Bisect the interval $[E_m, E_M]$ until the trial eigenvalue remains constant within the desired numerical accuracy. The estimate eigenvalue and eigenvector are E and $\psi(x)$, respectively.

The method presented here is almost complete, but it neglects a crucial property of the possible solutions of the initial value problem in the region where $V(x) > E$. Restricting for a moment to the simpler case of constant potential, in this region the Schrödinger equation reads:

$$\frac{1}{2}\frac{\mathrm{d}^2}{\mathrm{d}x^2}\psi_i(x) = k_i^2\psi_i(x), \quad k_i^2 = E - V > 0, \tag{C.6}$$

which implies $\psi_i(x) \approx \exp(\pm k_i x)$. Only one of these two solutions can be reconciled with the boundary conditions $\psi_i(x) \xrightarrow{|x|\to\infty} 0$, so we need to explicitly avoid the appearance of the non-normalizable solution in the integration of the differential equation. In order to avoid the exponential growth of the wave function, we integrate left-to-right from a to x_c, the "classical inversion point", $x_c \in I : V(x_c) = E$, and we then proceed to integrate the equation backwards from b towards x_c. We then match the value and the first derivative of the obtained function at x_c. Again counting the number of nodes and bisecting the interval until E stays constant within the desired accuracy yields the desired eigenvalue $E_i = E$ and the, now always normalizable, eigenstate $\psi_i(x) = \psi(x)$.

Appendix D

Prandtl-Tomlinson particle coupled to phonons

As a natural extension to the PT model considered in Chaps. **??** and **??**, we consider a quantum model composed of a harmonic chain of N particles interacting with a single particle ("the slider"), in a harmonic trap centered at position $\tilde{X}$. We denote operators referring to the slider with capital letters $\hat{X}$ and $\hat{P}$, and operators referring to the n-th particle in the chain with lower-case letters $\hat{x}_n$ and $\hat{p}_n$. If we denote by $V(X - x_n)$ a general interaction term between the slider and one of the particles in the chain, we can write Hamiltonian of the model as:

$$\hat{H}(\tilde{X}) = \frac{\hat{P}^2}{2M} + \frac{K}{2}(\hat{X} - \tilde{X})^2 + \sum_{n=1}^{N}\left[\frac{\hat{p}_n^2}{2m} + \frac{m\omega^2}{2}(\hat{x}_{n+1} - \hat{x}_n - a)^2\right] + \hat{V}_{\text{int}} \tag{D.1}$$

where:

$$\hat{V}_{\text{int}} = \sum_{n=1}^{N} V(\hat{X} - \hat{x}_n) \tag{D.2}$$

is the interaction potential between the slider and each bead in the harmonic chain, V being a sufficiently fast decaying function.

Assuming that chain displacements are small compared to the lattice spacing, and setting $\hat{x}_n = na + \hat{u}_n$, we can linearize the interaction:

$$\begin{aligned}\hat{V}_{\text{int}} = \sum_{n=1}^{N} V(\hat{X} - na - \hat{u}_n) &= \sum_{n=1}^{N}\Big(V(\hat{X} - na) - \hat{u}_n V'(\hat{X} - na) + \cdots\Big) \\ &\approx V_{\text{per}}(\hat{X}) - \sum_{n=1}^{N}\hat{u}_n V'(\hat{X} - na)\,,\end{aligned} \tag{D.3}$$

where

$$V_{\text{per}}(\hat{X}) = \sum_{n=1}^{N} V(\hat{X} - na) \tag{D.4}$$

is a periodic static potential experienced by the slider. Upon linearizing the

interaction, the Hamiltonian can be rewritten as follows:

$$\hat{H}(\tilde{X}) = \frac{\hat{P}^2}{2M} + \underbrace{\frac{K}{2}(\hat{X}-\tilde{X})^2 + V_{\rm per}(\hat{X})}_{V_{\rm PT}(\hat{X};\tilde{X})} + \sum_{n=1}^{N}\left[\frac{\hat{p}_n^2}{2m} + \frac{m\omega^2}{2}(\hat{u}_{n+1}-\hat{u}_n)^2\right] - \sum_{n=1}^{N}\hat{u}_n V'(\hat{X}-na)\ . \tag{D.5}$$

The partition function is:

$$\begin{aligned} Z(\tilde{X}) = \mathrm{Tr}\ \mathrm{e}^{-\beta\hat{H}(\tilde{X})} &= \int_{-\infty}^{\infty}\mathrm{d}X \int \prod_{n=1}^{N}\mathrm{d}u_n\ \langle X, u_1, \cdots u_N|\mathrm{e}^{-\beta\hat{H}(\tilde{X})}|X, u_1, \cdots u_N\rangle \\ &\equiv \int_{-\infty}^{\infty}\frac{\mathrm{d}X}{\lambda}\,\mathrm{e}^{-\beta F(X;\tilde{X})}\ , \end{aligned}$$

where $F(X;\tilde{X})$ is the constrained free-energy for the slider, and λ an appropriate length, e.g., the thermal wavelength Λ.

D.1 Integration of phonon variables

We now write the full partition function for the linearized Hamiltonian, using the imaginary-time path integral formalism, see Sec. **??** for an introduction. Our notation involves the various Trotter slice replicas. As before, $\mathbf{X} = (X_1, \cdots, X_P)$. We also denote as $\mathbf{u}_n = (u_{n,1}, \cdots, u_{n,P})$, and, collectively, $\mathbf{u}$ to be the $N \times P$ matrix with elements $u_{n,p}$. We can write:

$$Z(\tilde{X}) = \lim_{P\to\infty}\int\frac{\mathrm{d}\mathbf{X}}{\lambda_{T,s}^{P}}\int\frac{\mathrm{d}\mathbf{u}}{\lambda_{T,c}^{NP}}\,\mathrm{e}^{-\mathcal{A}(\mathbf{X},\mathbf{u};\tilde{X})}\ , \tag{D.6}$$

where:

$$\begin{aligned} \mathcal{A}(\mathbf{X},\mathbf{u};\tilde{X}) &= \mathcal{A}_s(\mathbf{X};\tilde{X}) + \mathcal{A}_c(\mathbf{u}) + \mathcal{A}_{sc}(\mathbf{X},\mathbf{u}) + \mathcal{A}_0 \\ \mathcal{A}_s(\mathbf{X};\tilde{X}) &= \frac{1}{2}\frac{2\pi P}{\lambda_{T,s}^2}\sum_{p=1}^{P}(X_{p+1}-X_p)^2 + \frac{\beta}{P}\sum_{p=1}^{P}V_{\rm PT}(X_p;\tilde{X}) \\ \mathcal{A}_c(\mathbf{u}) &= \frac{1}{2}\frac{2\pi P}{\lambda_{T,c}^2}\sum_{n=1}^{N}\sum_{p=1}^{P}(u_{n,p+1}-u_{n,p})^2 + \frac{\beta}{P}\frac{m\omega^2}{2}\sum_{n=1}^{N}\sum_{p=1}^{P}(u_{n+1,p}-u_{n,p})^2 \\ \mathcal{A}_{sc}(\mathbf{X},\mathbf{u}) &= -\frac{\beta}{P}\sum_{n=1}^{N}\sum_{p=1}^{P}u_{n,p}V'(X_p-na) \\ \mathcal{A}_0 &= -\frac{(N+1)P}{2}\log P\ . \end{aligned} \tag{D.7}$$

The terms $\mathcal{A}_c$ and $\mathcal{A}_{sc}$ of the action contain the phonon coordinates quadratically and linearly, respectively. $\mathcal{A}_c$ clearly shows a translational invariance on the "two-dimensional" coordinate grid (n,p) that suggests the use of lattice Fourier transforms. More precisely, if (n,p) denotes the direct lattice coordinates, we introduce reciprocal lattice wave-vectors $\mathbf{q} = (q_1, q_2)$ and the

Fourier transform:

$$u_{\mathbf{q}} = \frac{1}{\sqrt{NP}} \sum_{n=1}^{N} \sum_{p=1}^{P} u_{n,p}\, \mathrm{e}^{-i(q_1 n + q_2 p)} \tag{D.8}$$

with inverse given by:

$$u_{n,p} = \frac{1}{\sqrt{NP}} \sum_{\mathbf{q}}^{\mathrm{BZ}} u_{\mathbf{q}}\, \mathrm{e}^{i(q_1 n + q_2 p)} \ . \tag{D.9}$$

Notice that $u^*_{\mathbf{q}} = u_{-\mathbf{q}}$ since the $u_{n,p}$ are **real**. The NP wave-vectors $\mathbf{q}$ in the Brillouin Zone (BZ) are given by:

$$q_1 = \frac{2\pi l_1}{N} \ , \quad q_2 = \frac{2\pi l_2}{N} \quad \text{with} \quad l_1 = -\tfrac{N}{2}{+}1, \cdots, \tfrac{N}{2} \ ; \quad l_2 = -\tfrac{P}{2}{+}1, \cdots, \tfrac{P}{2} \ . \tag{D.10}$$

Next, by introducing the anisotropic spring constants (both with physical dimension of $1/\mathrm{length}^2$):

$$K_1 = \frac{\beta}{P} m\omega^2 \ , \qquad K_2 = \frac{2\pi P}{\lambda_{T,c}^2} \ , \tag{D.11}$$

we can rewrite the quadratic part (second line) of the action as:

$$\mathcal{A}_c(\mathbf{u}) = \frac{1}{2} \sum_{n=1}^{N} \sum_{p=1}^{P} \Big(K_1 (u_{n+1,p} - u_{n,p})^2 + K_2 (u_{n,p+1} - u_{n,p})^2 \Big) = \frac{1}{2} \sum_{\mathbf{q}}^{\mathrm{BZ}} \mathrm{D}_{\mathbf{q}} |u_{\mathbf{q}}|^2 \ , \tag{D.12}$$

where we introduced the Fourier transform of the dynamical matrix

$$\mathrm{D}_{\mathbf{q}} = 2K_1(1 - \cos q_1) + 2K_2(1 - \cos q_2) \geq 0 \ . \tag{D.13}$$

We now re-write the linear coupling term $\mathcal{A}_{sc}$ in Fourier transform:

$$\begin{aligned} \mathcal{A}_{sc} = -\frac{\beta}{P} \sum_{n=1}^{N} \sum_{p=1}^{P} u_{n,p} V'(X_p - na) &= -\frac{\beta}{P} \frac{1}{\sqrt{NP}} \sum_{\mathbf{q}}^{\mathrm{BZ}} u_{\mathbf{q}} \sum_{n=1}^{N} \sum_{p=1}^{P} \mathrm{e}^{i(q_1 n + q_2 p)} V'(X_p - na) \\ &= -\sum_{\mathbf{q}}^{\mathrm{BZ}} u_{\mathbf{q}} J^*_{\mathbf{q}} \ , \end{aligned} \tag{D.14}$$

where we have defined:

$$J_{\mathbf{q}} = \frac{\beta}{P} \frac{1}{\sqrt{NP}} \sum_{n=1}^{N} \sum_{p=1}^{P} \mathrm{e}^{-i(q_1 n + q_2 p)} V'(X_p - na) \ . \tag{D.15}$$

The goal is now to perform the Gaussian integral involving the phonon variables $\mathbf{u}$. Technically, full translational invariance in the Hamiltonian is broken by the position of the spring $\tilde{X}$. To prevent the slider to drag the whole chain along, we eliminate the uniform translation mode which gives a divergent contribution to the integral in Eq. (**??**). Notice also that the NP complex variables

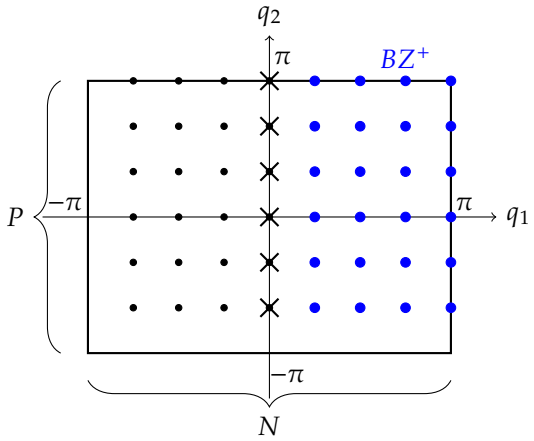

Figure D.1: A sketch of the Brillouin zone of the polymer.

$u_{\mathbf{q}}$ are not independent, since $u_{-\mathbf{q}} = u_{\mathbf{q}}^*$. Hence, we can concentrate on half of the BZ, where for every $\mathbf{q}$ we *do not include* the corresponding $-\mathbf{q}$: we denote this set of $\mathbf{q}$ vectors by BZ^+, see Fig. **??** for a depiction of this region of the Brillouin zone. The relevant integral is transformed as follows:

$$\int_{\mathbb{R}^{(N-1)P/2}\setminus\text{uniform}} \frac{\mathrm{d}^{(N-1)P/2}\mathbf{u}}{\lambda_{T,c}^{(N-1)P/2}}\, \mathrm{e}^{-\mathcal{A}_c(\mathbf{u})-\mathcal{A}_{sc}(\mathbf{X},\mathbf{u})} \tag{D.16}$$

$$\longrightarrow \frac{1}{\lambda_{T,c}^{(N-1)P/2}} \prod_{\mathbf{q}\neq\mathbf{0}}^{\mathrm{BZ}^+} \int \left[\mathrm{d}u_{\mathbf{q}}\mathrm{d}u_{\mathbf{q}}^*\right] \mathrm{e}^{-\mathrm{D}_{\mathbf{q}}|u_{\mathbf{q}}|^2+(u_{\mathbf{q}}J_{\mathbf{q}}^*+u_{\mathbf{q}}^*J_{\mathbf{q}})}$$

$$= \frac{1}{\lambda_{T,c}^{(N-1)P/2}} \prod_{\mathbf{q}\neq\mathbf{0}}^{\mathrm{BZ}^+} \frac{\pi}{\mathrm{D}_{\mathbf{q}}} \mathrm{e}^{|J_{\mathbf{q}}|^2/\mathrm{D}_{\mathbf{q}}} \,. \tag{D.17}$$

Observe the peculiar definition of the complex integral, where if $z = x + iy$:

$$\int [\mathrm{d}z\mathrm{d}z^*]\, f(z) \equiv \int \mathrm{d}x\mathrm{d}y\, f(x+iy) \,. \tag{D.18}$$

The final expression in Eq. (**??**) then follows from the standard real Gaussian integral:

$$\int \mathrm{d}x\, \mathrm{e}^{-Ax^2+xB} = \sqrt{\frac{\pi}{A}}\, \mathrm{e}^{B^2/(4A)} \,.$$

Notice that the vectors $\mathbf{q} \in \mathrm{BZ}^+ \setminus 0$ are exactly $(N-1)P/2$ in number, hence the normalization in Eq. (**??**) is correct, since $1/\mathrm{D}_{\mathbf{q}}$ has a dimension of length^2.

The substitution of the integrated phonon contribution Eq. (**??**) into Eq. (**??**) leads to an expression suitable for the calculation of equilibrium averages using the PIMC method, as described in Sec. **??**.